Are vapor-like fluids viable ore fluids for Cu-Au-Mo porphyry ore formation?

Nicole C. Hurtig[1*], Artas A. Migdisov[2] and Anthony E. Williams-Jones[3]

[1]Dept. of Earth and Environmental Science, New Mexico Tech, 801 Leroy Pl, Socorro, NM 87801, USA

[2]Earth and Environmental Division, Los Alamos National Laboratory, P.O. Box 1663, M.S. J535, Los Alamos, NM 87545, USA

[3]Dept. of Earth and Planetary Sciences, McGill University, University Street, Montreal, QC H3A, Canada

*corresponding author: nicole.hurtig@nmt.edu

Abstract

Ore formation in porphyry Cu-Au-(Mo) systems involves the exsolution of metal-bearing fluids from magmas and the transport of the metals in magmatic-hydrothermal plumes that are subject to pressure fluctuations. Deposition of ore minerals occurs as a result of cooling and decompression of the hydrothermal fluids in partly overlapping ore shells. In this study, we address the role of vapor-like fluids in porphyry ore formation through numerical simulations of metal transport using the Gibbs Energy Minimization Software, GEM-Selektor. The thermodynamic properties of the hydrated gaseous metallic species necessary for modeling metal solubility in fluids of moderate density (100 – 300 kg/m^3) were derived from the results of experiments that investigated the solubility of metals in aqueous HCl- and H_2S-bearing vapors. Metal transport and precipitation were simulated numerically as a function of temperature, pressure and fluid composition (S, Cl and redox). The simulated metal concentrations and ratios are compared to those observed in vapor-like and intermediate-density fluid inclusions from porphyry ore deposits, as well as gas

Hurtig, N. C., Migdisov, A. A., and Williams-Jones, A. E., 2021,
••Are Vapor-Like Fluids Viable Ore Fluids for Cu-Au-Mo Porphyry Ore Formation?
Economic Geology, v. 116, p. 1599-1624.

condensates from active volcanoes. The thermodynamically predicted solubility of Cu, Au, Ag and Mo decreases during isothermal decompression. At elevated pressure, the simulated metal solubility is similar to the metal content measured in vapor-like and intermediate-density fluid inclusions from porphyry deposits (at ~200-1800 bar). At ambient pressure, the metal solubility approaches the metal content measured in gas condensates from active volcanoes (at ~1 bar), which is several orders of magnitude lower than that in the high-pressure environment. During isochoric cooling, the simulated solubility of Cu, Ag and Mo decreases, whereas that of Au reaches a maximum between 35 ppb and 2.6 ppm depending on fluid density and composition. Similar observations are made from a compilation of vapor-like and intermediate-density fluid inclusion data showing that Cu, Ag and Mo contents decrease with decreasing P and T. Increasing the Cl concentration of the simulated fluid promotes the solubility of Cu, Ag and Au chloride species. Molybdenum solubility is highest under oxidizing conditions and low S content and gold solubility is elevated at intermediate redox conditions and elevated S content. The S content of the vapor-like fluid strongly affects metal ratios. Thus, there is a decrease in the Cu/Au ratio as the S content increases from 0.1 to 1 wt.%, whereas the opposite is the case for the Mo/Ag ratio; at S contents of >1 wt.%, the Mo/Ag ratio also decreases. In summary, thermodynamic calculations based on experiments involving gaseous metallic species predict that vapor-like fluids may transport and efficiently precipitate metals in concentrations sufficient to form porphyry ore deposits. Finally, the fluid composition and P-T evolution paths of vapor-like and intermediate-density fluids have a strong effect on metal solubility in porphyry systems and potentially exert an important control their metal ratios and zoning.

1. Introduction

Hurtig, N. C., Migdisov, A. A., and Williams-Jones, A. E., 2021,
••Are Vapor-Like Fluids Viable Ore Fluids for Cu-Au-Mo Porphyry Ore Formation?
Economic Geology, v. 116, p. 1599-1624.

Porphyry Cu-Au-Mo deposits represent the largest source of Cu and Mo ore world-wide and contain significant resources of Au, W, Re and Ag (Singer et al., 2005; Sinclair, 2007). They are associated with porphyritic intrusive complexes and form in the root zones of andesitic volcanoes in subduction-related, continental and island-arc settings (Sillitoe, 1973; 2010; Cooke et al., 2005; Sinclair, 2007; Richards, 2014). Although, economic porphyry deposits form mainly at shallow crustal levels, i.e., 2 to 5 km depth (Vila and Sillitoe, 1991; Proffett, 2009; Murakami et al., 2010; Schöpa et al., 2017), some, notably the Butte Deposit, occur at greater depth (>6 km; Rusk et al., 2008; Mercer and Reed, 2013) and others such as those of the Maricunga Belt, Chile (Muntean and Einaudi, 2000; 2001) and the Jarovie Belt, Slovakia (Koděra et al., 2014) that are emplaced at very shallow depth (< 2km). The economic mineralization is hosted mainly in quartz vein stockworks that provide evidence of a complex history of multiple episodes of veining, alteration and ore mineral deposition (Sillitoe, 1973; Gustafson and Hunt, 1975; Hedenquist et al., 1998; Rusk and Reed, 2002; Redmond et al., 2004; Landtwing et al., 2005; Rusk et al., 2008; Redmond and Einaudi, 2010; Sillitoe, 2010; Landtwing et al., 2010; Monecke et al., 2018).

Ore formation in porphyry systems (Fig. 1a, b) involves the exsolution of hydrothermal fluids in the cupolas of large-scale crustal batholiths and the transport of the metals upward and outward from the magmatic centers where they precipitate in overlapping ore shells upon cooling and decompression (Lowell and Guilbert, 1970; Gustafson and Hunt, 1975; Henley and McNabb, 1978; Dilles, 1987; Williams-Jones and Heinrich, 2005; Rusk et al., 2008; Richards, 2013). Commonly, a saline intermediate-density supercritical fluid exsolves from the magma and upon cooling and decompression separates into a low density vapor and a high density hypersaline liquid (Eastoe, 1978; Henley and McNabb, 1978; Bodnar and Beane, 1980; Hezarkhani and Williams-Jones, 1998; Redmond et al., 2004; Heinrich, 2005; Landtwing et al., 2005; Driesner and Heinrich,

Hurtig, N. C., Migdisov, A. A., and Williams-Jones, A. E., 2021,
••Are Vapor-Like Fluids Viable Ore Fluids for Cu-Au-Mo Porphyry Ore Formation?
Economic Geology, v. 116, p. 1599-1624.

2007; Lecumberri-Sanchez et al., 2015; Audétat, 2019; Mernagh et al., 2020). Upon separation of a moderately saline (2 - 8 wt.% NaCl) fluid the vapor dominates volumetrically over the hypersaline brine (Fig. 1b). For example, Lerchbaumer and Audétat (2012) show that the vapor to brine mass ratio at Alumbrera was 4 – 9, which translates to a volume proportion of 96 – 98% vapor. A similar conclusion was reached by Mernagh et al. (2020) based on enthalpy constraints (i.e., 90 – 98 % vapor). The vapor to liquid phase proportions vary as a function of salinity, T and P and consequently may change considerably over the life-time of an active hydrothermal plume (Landtwing et al., 2010). In shallow systems, the fluid exsolving from the melt may be vapor-like and coexist with halite, salt melts or brine (Muntean and Einaudi, 2000; 2001; Heinrich et al., 2004; Williams-Jones and Heinrich, 2005; Koděra et al., 2014). The path of fluid evolution varies depending on the depth at which the fluid exsolves from the melt, the composition and volume of the fluid(s) (e.g., salinity, CO_2 content), and the permeability of the host rocks (Heinrich et al., 2004; Redmond et al., 2004; Heinrich, 2005; Williams-Jones and Heinrich, 2005; Klemm et al., 2007; Driesner and Heinrich, 2007; Rusk et al., 2008; Redmond and Einaudi, 2010; Monecke et al., 2018).

Elevated concentrations of ore metals (10 – 4300 ppm Cu, 0.05 – 10 ppm Au, 2 – 190 ppm Ag and 1 – 290 ppm Mo) have been detected in vapor-like and intermediate-density fluid inclusions (Heinrich et al., 1999; Ulrich et al., 1999; Audétat et al., 2000; Ulrich et al., 2002; Rusk et al., 2004; Klemm et al., 2007; 2008; Zajacz et al., 2008; Audétat, 2010; Seo et al., 2011; 2012; Lerchbaumer and Audétat, 2013; Seo and Heinrich, 2013). The data referred to here are based on laser ablation inductively coupled plasma mass-spectrometer (LA-ICP-MS) measurements of the vapor in composite brine-vapor inclusion assemblages and vapor-like and intermediate-density fluid inclusions that homogenize to the vapor or by critical behavior, respectively (Electronic

Hurtig, N. C., Migdisov, A. A., and Williams-Jones, A. E., 2021,
••Are Vapor-Like Fluids Viable Ore Fluids for Cu-Au-Mo Porphyry Ore Formation?
Economic Geology, v. 116, p. 1599-1624.

Appendix B: all data including references). Here we loosely refer to these fluids as vapor-like fluids, with the emphasis placed on predicting metal transport in compressible fluids of low to intermediate density (i.e., 0.1 to 322 kg/m^3 in the pure H_2O system). Elevated metal concentrations have also been documented in high temperature (melt-)vapor-brine partitioning experiments (Frank et al., 2002; 2003; Pokrovski et al., 2005; Simon et al., 2005; 2006; 2007; 2008; Zajacz et al., 2008; 2010; 2011; 2012; 2017). They have likewise been documented in lower temperature vapor experiments (Migdisov and Williams-Jones, 2013; Hurtig and Williams-Jones, 2014a; 2014b; Migdisov et al., 2014). These studies establish a baseline for metal contents in vapor-like fluids, providing the fundamental evidence that vapor-like fluids can transport sufficient metals to be considered ore fluids.

Numerical simulations of the physical aspects of porphyry copper ore formation have demonstrated the transient nature of the fluid phase states and fluid miscibility within magmatic-hydrothermal fluid plumes (Gruen et al., 2012; Weis et al., 2012; 2014; Afanasyev et al., 2018). Key observations from these simulations in the NaCl-H_2O system are the occurrence of pressure fluctuations, the presence of compressible intermediate-density supercritical fluids, occasional formation of 'immobile' brine lenses and a correspondingly high proportion of vapor after phase separation. Processes such as fluid-rock interaction and mineral precipitation have not been considered in these physical models. Advanced coupled chemical and physical reactive transport simulations only have been performed for major elements (i.e., O, H, S, C, Ca, Na, Cl, K, Al, Ma and Si) and have not evaluated metal transport and precipitation (Yapparova et al., 2019). To date, the only ore metal for which solubility has been coupled to physical transport models is copper (Weis et al., 2012). Weis (2015) simulated the flow of multiphase variably miscible H_2O-NaCl fluids and predicted the formation of self-organizing plumes with a stable temperature front where

Hurtig, N. C., Migdisov, A. A., and Williams-Jones, A. E., 2021,
••Are Vapor-Like Fluids Viable Ore Fluids for Cu-Au-Mo Porphyry Ore Formation?
Economic Geology, v. 116, p. 1599-1624.

Cu deposition occurs as a result of efficient cooling of the hydrothermal plume by an overlying meteoric convection cell. Chemically more complex models simulating metal transport of porphyry ore formation (Heinrich et al., 2004; Heinrich, 2005; Reed et al., 2013) have used existing thermodynamic models for aqueous liquids (e.g., the HKF-model; Helgeson et al., 1981). These chemical models predict the development of alteration sequences due to fluid-rock interaction comparable to those observed in porphyry deposits.

Lastly, some thermodynamic studies have approached the system from the vapor-side using metal volatility to estimate ore precipitation from magmatic gases (Krauskopf, 1957; Krauskopf, 1964; Eastoe, 1982) and/or vapor-liquid partitioning data from experiments and vapor-melt partitioning data from active volcanoes (Pokrovski et al., 2013). These simulations have not yielded metal concentrations (i.e., Au, Cu, Ag and Mo) sufficient for ore formation by vapor-like fluids, because the solvating properties of water vapor were not considered (see Section 2, Hydration model, for more detail). The density-model (Marshall and Franck, 1981; Anderson et al., 1991; Akinfiev and Diamond, 2004) has yielded promising results for predicting Ag solubility in low-density fluids for a wide range of temperature and fluid density (Akinfiev and Zotov, 2016). As this model has not been implemented into a thermodynamic code package such as GEM-Selektor, it is currently not possible to use the density-model to simulate metal ratios and fluid-mineral reactions. In summary, existing models have failed to predict metal transport in multicomponent vapor-like aqueous fluids relevant to porphyry ore formation because of a paucity of experimental data for low- and intermediate-density fluids and the difficulty of introducing these data into thermodynamic code packages.

In Hurtig and Williams-Jones (2015), we presented a model for Au-Ag-Mo solubility designed specifically to treat the case of metal transport by vapor-like fluids based on experiments

Hurtig, N. C., Migdisov, A. A., and Williams-Jones, A. E., 2021,
••Are Vapor-Like Fluids Viable Ore Fluids for Cu-Au-Mo Porphyry Ore Formation?
Economic Geology, v. 116, p. 1599-1624.

(Migdisov et al., 1999; Archibald et al., 2001; Rempel et al., 2006; Zezin et al., 2007; 2011; Migdisov and Williams-Jones, 2013; Hurtig and Williams-Jones, 2014a; 2014b). Here, we expand on our earlier study by including experimental data for CuCl solubility in water vapor (Archibald et al., 2001; Migdisov et al., 2014). We present comprehensive thermodynamic simulations of the behavior of Cu, Au, Ag and Mo solubility in vapor-like fluids buffered by simplified vein gangue mineral assemblages using the GEM-Selektor code package (Kulik et al., 2013). These simulations approach the thermodynamic modelling from the gas phase; importantly we consider metal solubility as a function of water vapor pressure and hydrated gaseous species. Vapor-liquid partitioning is not simulated, and cooling paths only follow metal transport and precipitation from vapor-like fluids. Four numerical simulation setups (Fig. 1c) were employed to understand: 1) the effect of fluid chemistry on metal solubility and metal ratios at high temperature in a vapor-like fluid (i.e., titration of Cl, S and O); (2) the effect of isothermal decompression; (3) isochoric cooling on metal mobility and metal ratios and (4) single-pass flow-through ore formation and metal zoning models. We compare the simulated metal concentrations and ratios to those of vapor-like fluid inclusions, volcanic gas condensates and ores in porphyry deposits. Based on these comparisons, we evaluate the contributions of the simulated processes to metal enrichment and identify the key drivers of porphyry ore genesis within a magmatic-hydrothermal plume.

2. A hydration model for predicting gaseous metallic speciation

The role of water as a solvent is the key to understanding metal transport in aqueous fluids, which can be decompressed from a liquid-like to a vapor-like fluid density above the critical temperature and pressure of water without crossing any phase boundaries (Weingärtner and Franck, 2005). Water is an ideal solvent because it is a dipolar molecule with a high negative charge density near

the oxygen atom and a high positive charge density near the hydrogen protons (Weingärtner and Franck, 2005). It exists as a fluid (liquid or gas) over a wide range of temperature and pressure, and, in its liquid state, dipole-dipole interaction between water molecules leads to the formation of a strong network of hydrogen bonds (Franks, 1973). This network is responsible for the physicochemical properties of liquid water, the formation of water clusters and hydration shells around ions and other dipole molecules and the dissociation of aqueous species (Dagade and Barge, 2016). These are essential characteristics of liquid water and control its capacity to dissolve solutes, notably those forming ionic (charged) species. In the most widely used model for the thermodynamic prediction of element transport by aqueous liquid, the HKF model (Helgeson et al., 1981), the capacity of water for ion association/dissociation at any given temperature, pressure and density is described by the Born equation (Born, 1920; Bucher and Porter, 1986; Majer et al., 2008). The Born equation is used to estimate the electrostatic component of the Gibbs free energy of solvation of an ion of a given charge and radius. It is an electrostatic model that treats water as a continuous dielectric medium having a physical state that is an incompressible continuum. This equation and, by extension, the HKF model, accurately predicts metal solubility in electrolyte solutions with liquid-like density at low to moderate temperature but fails to predict metal transport in non-electrolyte solutions with vapor-like density.

In the gas state, the dielectric constant decreases exponentially with decreasing water vapor density and increasing temperature (Fernández et al., 1997). Consequently, in vapor-like fluids the dielectric constant is low and ion association is strong, thereby stabilizing neutral compounds at the expense of ionic species. Like liquid water, water vapor is composed of polar molecules and can therefore dissolve solids (Weingärtner and Franck, 2005). Thus, the solubility of oxides (e.g., SiO_2, MoO_3 and WO_3) in water vapor is orders of magnitude higher than their volatility in dry gas,

Hurtig, N. C., Migdisov, A. A., and Williams-Jones, A. E., 2021,
••Are Vapor-Like Fluids Viable Ore Fluids for Cu-Au-Mo Porphyry Ore Formation?
Economic Geology, v. 116, p. 1599-1624.

i.e., the vapor pressure over the corresponding solid (Hannay et al., 1880; Morey and Hesselgesser, 1951; Morey, 1957; Wendlandt and Glemser, 1964). The importance of hydrated gaseous species was first recognized by Pitzer and Pabalan (1986), for the NaCl-H_2O system. The solubility of NaCl in water vapor and liquid was subsequently modeled for a wide range of temperature and pressure, and shown to increase continuously from vapor to liquid in supercritical fluids (Bischoff et al., 1986; Pitzer et al., 1987; Tanger and Pitzer, 1989; Sterner et al., 1992; Anderko and Pitzer, 1993). A solubility continuum in supercritical fluids also has been demonstrated for copper. This was done using synchrotron X-ray absorption spectroscopic (XAS) techniques in S-free and S-bearing solutions (Liu et al., 2008; Etschmann et al., 2010; Louvel et al., 2017). The same continuum for Mo had been demonstrated using the solubility method (Wendlandt and Glemser, 1964; Hurtig and Williams-Jones, 2014a). The increase in metal solubility with water density is related to the formation of metal-water and water-water molecule clusters (Fig. 2) and has been simulated using *ab initio* molecular dynamics and density functional theory (Godinho et al., 2005; Mei et al., 2014; 2018). Thus, metal solubility in vapor-like fluids may be viewed as a series of hydration steps with increasing hydration number for which the free energy can be calculated from experimental data or predicted by theory. For hydration numbers below two, metal solubility (Au, Ag, Mo and Cu) is dominated by solute-solvent interaction and consequently is heavily influenced by the electronic structure of the corresponding volatile metallic species (Fig. 2b). The latter, in turn, is reflected by differences in the enthalpy and entropy of hydration for these species. For hydration numbers above two, the contribution of solute-solvent interaction decreases sharply with increasing hydration number and solvent-solvent interaction dominates (Fig. 2b). Thus, above a hydration number between 3 and 6, which depends on the metal of interest (Au, Ag, Cu and Mo), the energy of hydration (per water molecule added) approaches a constant similar to that calculated

Hurtig, N. C., Migdisov, A. A., and Williams-Jones, A. E., 2021,
••Are Vapor-Like Fluids Viable Ore Fluids for Cu-Au-Mo Porphyry Ore Formation?
Economic Geology, v. 116, p. 1599-1624.

using theoretical models for water molecule cluster formation (Mejías and Lago, 2000; Velizhanin et al., 2020). Below, we use the observations described above to simulate metal transport in the continuum between vapor-like fluids and those of intermediate density.

3. Methods

3.1 The thermodynamic framework

The sources of the thermodynamic data for the minerals and gases used in the numerical simulations are summarized in Tables A1-3 (Electronic Appendix A) and were managed with the GEM-Selektor code package (Karpov et al., 2001, 2002; Kulik et al., 2013). Data for the minerals were compiled from Johnson et al. (1992), Robie and Hemingway (1995), Chase (1998), Evans et al., (2010) and Holland and Powell (1998; 2011) and temperature-dependent phase transitions for the sulfides at the conditions of interest were implemented (entropy, enthalpy, volume and c_p-function). Data for the heat capacity and enthalpy of the phase transition for acanthite were taken from Grønvold and Westrum (1986) and for bornite, chalcopyrite and chalcocite from Robie et al. (1994). Thermodynamic data for the major gases, H_2O_g, $H_{2,g}$, $CO_{2,g}$, $CH_{4,g}$, CO_g, $Cl_{2,g}$, $O_{2,g}$, HCl_g, H_2S_g, and $SO_{2,g}$ were compiled from Frenkel (1994), Robie and Hemingway (1995) and Chase (1998) and parameters for the Peng-Robinson-Stryjek-Vera (PRSV) equation of state were taken from Proust and Vera (1989) and Stryjek et al. (1986).

The gaseous metallic species considered in this study, were limited to Au, Ag, Mo and Cu for which experimental data are available. The experimental data for the metallic gaseous species were fitted using the linear relationship of log K_s to the inverse of temperature and the species were added as reaction-dependent components in GEM-Selektor. The fitted parameters for the hydrated gold chloride species, $AuCl(H_2O)_y$, were taken from Hurtig and Williams-Jones (2014b) and for

Hurtig, N. C., Migdisov, A. A., and Williams-Jones, A. E., 2021,
••Are Vapor-Like Fluids Viable Ore Fluids for Cu-Au-Mo Porphyry Ore Formation?
Economic Geology, v. 116, p. 1599-1624.

hydrated molybdenum trioxide, $MoO_3(H_2O)_y$ from Hurtig and Williams-Jones (2014a). Experimental data for the hydrated silver chloride species, $AgCl(H_2O)_y$ (Migdisov et al., 1999; Migdisov and Williams-Jones, 2013) and for solvated gold sulfide species, $AuS(H_2S)_{x-1}(H_2O)_y$ (Zezin et al., 2007; Zezin et al., 2011), were fitted in Hurtig and Williams-Jones (2015). Experimental data for solvated copper chloride species, $CuCl(H_2O)_y$ and $CuCl(HCl)(H_2O)_y$ (Archibald et al., 2002; Migdisov et al., 2014) were fitted in this study (Table A2). The experimental data for AgCl, CuCl and AuS species were refitted for consistent implementation into GEMS. Details of the fitting these experimental data and the validity range of all gaseous hydrated metallic species used in this study can be found in the Electronic Appendix A.

The activity models and equations of state are summarized in the TSolMod library class (Wagner et al., 2012). The reference state is 25 °C and 1 bar. The standard state for all solids was that of a pure phase and for the gases was that of an ideal gas at 1 bar. A sub-regular solid-solution model for Au-Ag alloys (White et al., 1957) was introduced as a set of user-defined temperature-dependent equations (see Electronic Appendix A for details). In the gas-mineral equilibrium simulations, all gases were treated as ideal and ideal mixtures (see 6.4). This is currently a limitation of the GEM-Selektor code package, which cannot treat non-ideal gas mixtures with reaction-dependent components, our only method for implementing the experimentally derived gaseous metallic species. The experimental data for the metallic gaseous species were fitted to water fugacity and thus were modeled at water fugacity instead of total pressure (see Electronic Appendix A for pressure tables using IAPW-95). This adaptation was necessary to preserve the observed exponential increase in solubility of the metallic gaseous species (Fig. 3) with water vapor density and to ensure that the correct P-T behavior of these species was modeled. The

Hurtig, N. C., Migdisov, A. A., and Williams-Jones, A. E., 2021,
••Are Vapor-Like Fluids Viable Ore Fluids for Cu-Au-Mo Porphyry Ore Formation?
Economic Geology, v. 116, p. 1599-1624.

simulated metal solubility was tested against the experimental data and was reproducible within the experimental uncertainty (see Electronic Appendix A and Table A3).

3.2 Numerical simulations

The geochemical simulations of the behavior of Ag-Au-Cu-Mo-bearing vapors were carried out using GEM-Selektor v.3.7 (http://gems.web.psi.ch/GEMS3/), which employs a Gibbs energy minimization approach (Karpov et al., 2001, 2002; Kulik et al., 2013). We present four numerical simulations (Fig. 1c), namely 1) titration at constant (high) temperature and pressure with variable fluid chemistry 2) isothermal decompression, 3) isochoric cooling and 4) single-pass flow-through reaction. The titration models at constant temperature and pressure evaluate the effects of S, Cl and the redox condition on the solubility of the ore-forming minerals. The isothermal decompression models show the solubility as a function of fluid density, providing a connection between the conditions of volcanic gases (~1 bar) and those of porphyry systems (100 – 1800 bar). The isochoric cooling models evaluate the mobility of ore metals along a constant-density fluid evolution path. The simulated P-T paths only consider the vapor-path after phase separation i.e., the aqueous liquid was not activated/considered in these simulations. Thus, by not considering the liquid, the conditions minimized metal solubility and maximized mineral precipitation from vapor-like fluids. The single-pass flow-through reaction simulations represents the progressive reaction of a batch of vapor-like fluid with buffer minerals while simultaneously cooling and decompressing. This model was used to investigate metal zoning. The modeling conditions are summarized in Table 2.

The titration models at 600 ºC and 810 bar (density of 300 kg/m^3) involved ore mineral saturation and were conducted at varying redox conditions and for variable S and Cl contents (Fig.

Hurtig, N. C., Migdisov, A. A., and Williams-Jones, A. E., 2021,
••Are Vapor-Like Fluids Viable Ore Fluids for Cu-Au-Mo Porphyry Ore Formation?
Economic Geology, v. 116, p. 1599-1624.

1c). In order to select realistic concentration ranges for major components in the simulations, we turned to the compositional data available for volcanic gases and vapor-like and intermediate-density fluid inclusions from porphyry deposits (Table 3; see Electronic Appendix B for individual data sets and references). The S (SO_2 and H_2S), Cl (HCl) and C (CO_2) contents of volcanic gases range widely, from 0.002 – 26 wt.%, 0.002 – 16 wt.% and 0.02 – 55 wt.%, respectively (Gemmell, 1987; Symonds et al., 1987; 1990; Giggenbach and Matsuo, 1991; Symonds et al., 1992; Hedenquist et al., 1994; Symonds et al., 1994; Taran et al., 1995; Giggenbach, 1996; Symonds et al., 1996; Taran et al., 2000; 2001; Scher et al., 2013; Zelenski et al., 2014; Taran and Zelenski, 2015 and references therein; Nadeau et al., 2016). The ranges in the concentrations of these components reported for vapor-like and intermediate-density fluid inclusions from porphyry deposits are similar, namely 0.1 – 1.3 wt.% S, 1.0 – 8.9 wt.% Cl and 1.1 – 13 wt.% C (Ulrich et al., 1999; Audétat et al., 2000; Ulrich et al., 2002; Tarkian et al., 2003; Redmond et al., 2004; Rusk et al., 2004; Klemm et al., 2007; 2008; Rusk et al., 2008; Zajacz et al., 2008; Seo et al., 2009; Audétat, 2010; Landtwing et al., 2010; Seo et al., 2012; Lerchbaumer and Audétat, 2013; Seo and Heinrich, 2013; Audétat, 2019; Zaheri-Abdehvand et al., 2020). Major element compositions considered in the simulations range from 0.0002 – 10 wt.% S and 0.01 – 1 wt.% Cl, the C content was held constant at 2 wt.%, which is the median value for high T vapor-like and intermediate-density porphyry fluids see Table 3 (see Electronic Appendix B).

Measuring the sulfur content of fluid inclusions is challenging and consequently only a modest data set is available. From our simulations (see 5.1) it is apparent that the amount of S in the fluid exercises an important control on metal ratios. Therefore, we decided to expand the range of S contents to data from volcanic gases. The Cl range chosen for our simulations is narrower than that reported by Audétat (2019) for single-phase ore fluids (5 to 15 wt.% NaCl). Our compilation

Hurtig, N. C., Migdisov, A. A., and Williams-Jones, A. E., 2021,
••Are Vapor-Like Fluids Viable Ore Fluids for Cu-Au-Mo Porphyry Ore Formation?
Economic Geology, v. 116, p. 1599-1624.

of fluid inclusion data returned a range of 1 – 9 wt. % NaCl, averaging 4.4 wt.% NaCl (i.e., 2.9 wt.% Cl), because we excluded single-phase fluids with a liquid-like density. In the simulations, we further reduced this amount of Cl by ignoring Cl that would have complexed with Na, K, Fe, and thus not have been available for complexation with Au, Ag and Cu.

The redox condition was described as the redox potential, $R_H = \log (f_{H2}/f_{H2O})$, which represents the most meaningful probe into the redox states of volcanic gases (Giggenbach, 1987; 1996). In Electronic Appendix B, we also report the sulfidation potential (Einaudi et al., 2003) as $R_S = \log (f_{H2}/f_{H2S})$. The use of the Gibbs Energy Minimization method in GEM-Selektor allowed for evaluation of the redox potential for each local equilibrium step, by varying the amount of $H_{2,gas}$ and $O_{2,gas}$ in the vapor-like fluid. All simulations were performed in the vapor-solid system and by employing vapor-mineral equilibria in which the mineral assemblage changed from the reducing assemblage, calcite-ilmenite-magnetite(±pyrrhotite) to the oxidizing assemblage, hematite-anhydrite-rutile(±pyrite). Owing to the lack of direct measurements of redox sensitive species in fluid inclusions, the redox potential of porphyry-ore forming fluids can only be estimated (see Section 4).

We present two types of cooling and decompression simulations (Fig. 1c), namely isothermal decompression and isochoric cooling (red and orange pathways in Fig. 4h), at ore mineral saturation. Isothermal decompression was simulated for three temperatures (600, 400 and 300 ºC), constant Cl concentration (500 ppm) and two S contents (0.1 and 5.5 wt.%). Isochoric cooling (600 to 180 ºC) was modeled for a constant Cl content (500 ppm), S contents of 0.2 and 5.5 wt.% and a density of 300 and 100 kg/m^3. The isochoric cooling pathways modeled in this study represent projections of a plausible P-T fluid pathway recorded in fluid inclusion data projected from the NaCl-H_2O system to that of pure water (red and orange paths in Fig. 4h; Electronic

Hurtig, N. C., Migdisov, A. A., and Williams-Jones, A. E., 2021,
••Are Vapor-Like Fluids Viable Ore Fluids for Cu-Au-Mo Porphyry Ore Formation?
Economic Geology, v. 116, p. 1599-1624.

Appendix A). Below the critical point of water, the vapor density corresponds to that of water vapor at the water vapor saturation pressure. The pressure in these simulations was expressed as a temperature-dependent user-defined polynomial function (see Electronic Appendix A).

Ore mineral precipitation during cooling and decompressing was modeled using a single-pass flow-through reaction simulations (Fig. 1c). The metal ratios of the simulated fluids were taken from the compositional models at 600 ºC, 810 bar and a density of 300 kg/m^3. These fluids were slightly undersaturated with respect to the ore minerals, molybdenite, electrum, chalcopyrite, bornite, chalcocite, acanthite (see Table 4 for starting fluid compositions). Because we used the metal ratios determined in the titration models and employed a similar degree of undersaturation, the ore precipitation models clearly illustrate the effects of the initial S, Cl and R_H fluid composition on the P-T evolution paths. The fluids become saturated during cooling and decompression and precipitate ore minerals during each step while equilibrating with a constant buffer mineral assemblage needed to constrain the redox potential of the evolving fluid (see Section 4). The simulated fluid varied compositionally from 0.05 – 10 wt.% Cl, 0.1 – 3 wt.% S, -3.2 – 4.0 R_H at 2 wt.% C. In simulations at 1 and 10 wt.% Cl, the HCl/$\sum$Cl ratio provides a measure of the excess Cl and illustrates the control on metal zonation with various degrees of ore mineral undersaturation in the starting fluid. User-defined GEM-Selektor scripts and additional information on the modeling setup can be found in the Electronic Appendix A and B.

4. Mineral-gas reactions in numerical simulations

Mineral-gas buffering is a widely used concept involving the interaction of a gas with minerals and has been employed frequently to describe active geothermal and volcanic gas systems (Giggenbach, 1981; Stefánsson and Arnórsson, 2002; Henley and Seward, 2018). The concept is

Hurtig, N. C., Migdisov, A. A., and Williams-Jones, A. E., 2021,
••Are Vapor-Like Fluids Viable Ore Fluids for Cu-Au-Mo Porphyry Ore Formation?
Economic Geology, v. 116, p. 1599-1624.

based on the exchange of elements between minerals and gases as these phases adjust their compositions during the attainment of a steady state ('equilibrium'). In a multicomponent system, the redox potential and S content of the gas are controlled by several competing mineral-gas reactions and thus can only be described in terms of boundary conditions (i.e., minimum and maximum values) and not a single value (e.g., those of the hematite-magnetite or nickel-nickel oxide buffers, Fig. 5).

The application of mineral-gas buffers in our numerical simulations was essential in providing a basis for relating the simulated fluids to natural ore-forming systems, because they allowed us to realistically evaluate the redox condition and S contents for different parts of the porphyry ore-forming environment. The vapor-like fluid (H-O-S-Cl-C-Au-Ag-Mo-Cu) is equilibrated with solid phases that also include Ca, Fe and Ti (Table 1A in Electronic Appendix A). We currently cannot simulate the mobility of Ca, Fe, and Ti in vapor-like fluids due to a lack of thermodynamic data for species involving these elements. Thus, the model assumes that Ca, Fe and Ti are only present in the minerals that buffer the vapor-like fluid and are present at all conditions, whereas ore-forming metals (Au, Ag, Mo and Cu) are mobile. In porphyry ore deposits, Ca occurs as anhydrite, plagioclase and apatite, Ti as rutile/anatase, titanite or as a trace component in biotite and quartz and Fe occurs as magnetite, hematite, biotite and various Fe- and Fe-Cu-sulfides. These minerals are abundantly present in porphyry deposits as documented by numerous petrographic studies (Lowell and Guilbert, 1970; Sillitoe, 1973; Gustafson and Hunt, 1975; Hedenquist et al., 1998; Rusk and Reed, 2002; Redmond et al., 2004; Landtwing et al., 2005; Rusk et al., 2008; Redmond and Einaudi, 2010; Sillitoe, 2010; Landtwing et al., 2010; Richards, 2014; Zaheri-Abdehvand et al., 2020).

Hurtig, N. C., Migdisov, A. A., and Williams-Jones, A. E., 2021,
••Are Vapor-Like Fluids Viable Ore Fluids for Cu-Au-Mo Porphyry Ore Formation?
Economic Geology, v. 116, p. 1599-1624.

The following list of simplified mineral-gas and gas-gas reactions buffer the boundary conditions for the simulated vapor-like fluids:

Anhydrite-Calcite:	$CaCO_{3,s} + H_2O_g + \mathbf{SO_{2,g}} = CaSO_{4,s} + \mathbf{CO_{2,g}} + \mathbf{H_{2,g}}$	(1)
Rutile-Magnetite-Ilmenite:	$3TiO_{2,s} + Fe_3O_{4,s} + \mathbf{H_{2,g}} = 3FeTiO_{3,s} + H_2O_g$	(2)
Magnetite-Pyrite:	$Fe_3O_{4,s} + \mathbf{6H_2S_g} = 3FeS_{2,s} + 4H_2O_g + \mathbf{2H_{2,g}}$	(3)
Hematite-Magnetite:	$3Fe_2O_{3,s} + \mathbf{H_{2,g}} = 2Fe_3O_{4,s} + H_2O_g$	(4)
Pyrite-Pyrrhotite:	$FeS_{2,s} + \mathbf{H_{2,g}} = FeS_s + \mathbf{H_2S_g}$	(5)
S-gas buffer:	$SO_{2,g} + \mathbf{3H_{2,g}} = H_2S_g + 2H_2O_g$	(6)

The range of redox conditions covered by these mineral and gas buffers represent R_H values between the nickel-nickel oxide, the quartz-magnetite-fayalite and the hematite-magnetite buffer (Fig. 5a). Based on petrographic analysis of the deep barren stockwork zone of porphyry deposits we can associate the assemblage magnetite-anhydrite-rutile with porphyry ore formation (Macdonald and Arnold, 1994; Audétat et al., 2004; Reed et al., 2013). This mineral assemblage is stable at R_H values ranging between -3.6 and -4.1 at S contents below pyrite saturation (<4.8 wt.% S), thus providing a relatively well constrained field for R_H values for a typical porphyry ore fluid in equilibrium with magnetite, anhydrite and rutile. The R_H porphyry field is constrained by Equation 4 (hematite-magnetite) towards more oxidizing conditions and by Equation 2 (rutile-magnetite-ilmenite) towards more reducing conditions. The reducing boundary condition is expanded in pyrite saturated simulations to R_H values of -3.0 bounded by Equation 5. The R_H conditions identified here overlap with predicted f_{O2}-T ranges in Richards (2014), which indicate

Hurtig, N. C., Migdisov, A. A., and Williams-Jones, A. E., 2021,
••Are Vapor-Like Fluids Viable Ore Fluids for Cu-Au-Mo Porphyry Ore Formation?
Economic Geology, v. 116, p. 1599-1624.

that porphyry Cu-Au ore formation is favored by the H_2S-SO_2 gas buffer over more reducing mineral buffers.

The dominant Fe-bearing mineral assemblage affects the stability field of Fe^{2+}-bearing minerals and constrains R_H values relevant for porphyry ore forming fluids. The only other Fe-bearing mineral phase occurring in high-temperature porphyry alteration zones is biotite, which contains Fe^{2+} and/or Fe^{3+} and, for simplification, was not simulated in this study. Simulations designed to investigate the redox potential in silicate-bearing systems (Electronic Appendix B) predict mineral assemblages typical of the high temperature stage of porphyry deposit evolution (biotite, k-feldspar, plagioclase, quartz, andalusite, magnetite, rutile, anhydrite). The R_H values of these simulations are -3.3 and -4.2, which are within the range represented by the simplified assemblages that exclude silicate phases.

The S content of the fluid is reflected in the mineral buffering assemblage through saturation of different S-bearing minerals. At low S content (~0.09 wt.%), anhydrite becomes stable over calcite in a fluid with 2 wt.% C (~7 wt.% CO_2) and in the Si-bearing calculations anhydrite is stable at ppt levels of S in vapor-like fluids (Electronic Appendix B). At a high S content (>4.8 wt.%), pyrite and pyrrhotite are stabilized over magnetite. This reaction is also observed in simulations involving silicates, for which the S content is >4.6 wt.% (see Electronic Appendix B). These reactions constrain the S content of vapor-like fluids with R_H values ranging between -3.0 and -4.1. As explained above, a typical high temperature porphyry mineral assemblage includes magnetite, anhydrite and rutile, whereas pyrite and pyrrhotite are generally not present. Nonetheless, inclusions of intermediate and monosulfide solid solutions (iss and mss) have been observed in magmatic minerals from several porphyry ore deposits and active volcanic analogues (Halter et al., 2002; 2005; Nadeau et al., 2010; Wilkinson, 2013; Richards, 2014;

Hurtig, N. C., Migdisov, A. A., and Williams-Jones, A. E., 2021,
••Are Vapor-Like Fluids Viable Ore Fluids for Cu-Au-Mo Porphyry Ore Formation?
Economic Geology, v. 116, p. 1599-1624.

Nadeau et al., 2016; Rottier et al., 2019). The presence of these high temperature sulfide phases is attributed to sulfide saturation in silicate melts. In the context of the simulations presented here, the occurrence of pyrite and pyrrhotite in the buffering mineral assemblage may be viewed as being representative of magmatic sulfide saturation during the exsolution aqueous fluids.

5. Numerical simulation results

5.1 Effect of fluid composition on ore metal solubility and metal ratios

The titration models were designed to determine the controls of Cl, S and redox conditions on metal solubility and metal ratios in vapor-like porphyry ore fluids. The titration models were performed at 600 ºC and 810 bar (i.e., a density of 300 kg/m^3) to represent the conditions of a high temperature vapor-like fluid after it had exsolved from a magma (Fig. 1). The fluid was saturated with ore minerals and buffered by various Ca, Ti and Fe minerals. The results of these simulations are summarized in Table 5, Figures 6-8 and the Electronic Appendix B.

The effect of Cl was modeled by progressively increasing the Cl content in the gas from 0.01 to 1.0 wt.% at a constant S concentration of 0.2 wt.% and 5.5 wt.%, respectively (Fig. 6). The simulated Cl contents (0.01 – 1.0 wt.%) overlap with the range of Cl concentrations measured in volcanic gases (0.002 – 16.3 wt.% Cl) and in NaCl-bearing vapor-like and intermediate-density inclusions from porphyry ore deposits (0.6 – 9.3 wt.% Cl; Table 3). Although at the lower end of the Cl concentration range for fluid inclusions, the simulated contents are considered to be realistic, as only a small proportion of the Cl in the porphyry fluids is available for complexation with Cu, Au and Ag. Thus, the Cl content used in this model can be considered equivalent to the excess Cl in the form of HCl (i.e., the Cl not complexed with Na, K, and Fe) in porphyry ore fluids. For example, for a total chlorinity of 5 wt.% NaCl equiv. at 0.01 HCl/∑Cl, the HCl content is 0.05

Hurtig, N. C., Migdisov, A. A., and Williams-Jones, A. E., 2021,
••Are Vapor-Like Fluids Viable Ore Fluids for Cu-Au-Mo Porphyry Ore Formation?
Economic Geology, v. 116, p. 1599-1624.

435 wt.%, and for 0.1 HCl/∑Cl, the HCl content is 0.5 wt.%. Numerical simulations conducted at
436 higher Cl contents result in orders of magnitude higher simulated metal solubility, greatly
437 exceeding reliably measured metal contents in vapor-like and intermediate-density fluid inclusions
438 (Table 3). The buffering mineral assemblage was magnetite-anhydrite-rutile for the low S model
439 (Fig. 6a) and pyrite-anhydrite-rutile for the sulfide-saturated model (Fig. 6d). Gaseous metal
440 chloride species of Cu, Ag and Au increase in concentration with increasing Cl content, whereas
441 concentrations of Mo and the AuS species remain constant (Fig. 6b, e). The Cu/Mo and Cu/Au
442 ratios increase with increasing Cl content (Fig. 6c, f).

443 To investigate the effect of S on metal solubility, the S content of the fluid was increased
444 progressively from 0 to 10 wt.% at constant Cl concentrations of 500 ppm and 0.3 wt.% (Fig. 7).
445 The gas phase was initially buffered by the assemblage magnetite-anhydrite-rutile at low S
446 contents. The redox conditions between ~0.5 and ~1.7 wt.% S were buffered mainly by hematite,
447 whereas between ~1.7 and 4.8 wt.% S magnetite was the dominant buffer. At higher S contents (>
448 4.8 wt.%), pyrite stabilized at the expense of magnetite. The replacement of magnetite by pyrite
449 as the main redox buffering mineral represents an upper limit for the S content of a porphyry ore
450 fluid buffered by the assemblage magnetite-anhydrite-rutile (Fig. 7a, d). The lower limit for the S
451 content of porphyry fluids is controlled by Reaction (1), which converts calcite to anhydrite.
452 Anhydrite became stable when the S content of the gas reached ~0.01 wt.% S at 2.0 wt.% C. This
453 range of S contents (0.01 – 4.8 wt.%) is within that observed in volcanic gases (0.004 – 25 wt.%
454 S) and overlaps with the range of S contents measured in fluid inclusions (0.17 – 1.3 wt.% S) from
455 porphyry ore deposits (Table 3). Copper and Ag concentrations decreased slightly with increasing
456 S content (Fig. 7b, e). Molybdenum concentrations decrease sharply with increasing S content,
457 whereas Au concentrations increase with S contents due to the importance of AuS (short for

Hurtig, N. C., Migdisov, A. A., and Williams-Jones, A. E., 2021,
••Are Vapor-Like Fluids Viable Ore Fluids for Cu-Au-Mo Porphyry Ore Formation?
Economic Geology, v. 116, p. 1599-1624.

458 $AuS(H_2S)_{x-1}(H_2O)_y$) species. Consequently, the Cu/Au ratio decreased with increasing S content
459 and the Cu/Mo ratio increased (Fig. 7c, f).

460 The effect of the redox condition, $R_H = \log(f_{H2}/f_{H2O})$, was evaluated for three different fluid
461 compositions (Table 2; Fig. 8). The low S model (0.1 wt.%; Fig. 8a) was simulated for two Cl
462 contents (500 ppm and 0.3 wt.%; Fig. 8b, c) and the sulfide-saturated model (5.5 wt.%; Fig. 8d)
463 was simulated for low Cl concentration (500 ppm; Fig. 8e). In the low S model, the buffering
464 mineral assemblage evolved with increasing $O_{2,g}$ content of the fluid from calcite-ilmenite-
465 magnetite, through magnetite-anhydrite-rutile to hematite-anhydrite-rutile (Fig. 8a). In the sulfide-
466 saturated model, the evolution of the buffering mineral assemblages was from calcite-rutile-
467 pyrrhotite through anhydrite-rutile-pyrite(-magnetite) to hematite-anhydrite-rutile (Fig. 8a).
468 Molybdenum concentration decreased by 3 – 7 orders of magnitude under reducing conditions,
469 whereas Cu and Ag contents remained roughly constant (Fig. 8b, c, e). The Au solubility reached
470 a maximum at conditions buffered by magnetite-anhydrite-rutile in the low S model and anhydrite-
471 rutile-pyrite(-magnetite) at sulfide-saturated conditions (Fig. 8b, c). At a constant Cl content of
472 500 ppm, the Cu/Au ratio was ~2 orders of magnitude lower in the sulfide-saturated model than in
473 the low S model (Fig. 8f). However, the Cu/Au ratio increased by only ~0.2 orders of magnitude
474 in the low S models in response to an increase in the Cl concentration from 500 ppm to 0.3 wt.%
475 (Fig. 8f). The Cu/Mo ratio decreased by 4 – 6 orders of magnitude for the oxidized mineral
476 assemblage relative to the reduced mineral assemblage (Fig. 8g). There was also a large increase
477 in the Cu/Mo ratio (1 – 4 orders of magnitude) from the low S to the sulfide-saturated model; the
478 corresponding increase from the low to the high Cl model was only 1 – 2 orders of magnitude.
479

480 5.2 Isothermal Decompression

Hurtig, N. C., Migdisov, A. A., and Williams-Jones, A. E., 2021,
••Are Vapor-Like Fluids Viable Ore Fluids for Cu-Au-Mo Porphyry Ore Formation?
Economic Geology, v. 116, p. 1599-1624.

The isothermal decompression models were developed to better understand the effects of pressure fluctuation and decompression on metal solubility in magmatic-hydrothermal systems. In porphyry ore deposits, pressure fluctuations are well documented by fluid inclusion data (Heinrich et al., 1999; Audétat et al., 2000a; Ulrich et al., 2002, 1999; Klemm et al., 2007; Zajacz et al., 2008; Seo et al., 2012, 2011; Lerchbaumer and Audétat, 2013; Mercer and Reed, 2013; Seo and Heinrich, 2013), multi-generational quartz textures (Rusk and Reed, 2002; Landtwing et al., 2005; Monecke et al., 2018) and studies of vein density and geometry (Gruen et al., 2010).

The vapor-like fluid was saturated with ore minerals during decompression at 600 ºC from 810 to 10 bar, at 400 ºC from 296 bar to 10 bar, and at 300 ºC from the water vapor saturation pressure to 10 bar. The low S model was buffered by the mineral assemblage, magnetite-anhydrite-rutile, and the sulfide-saturated model by magnetite-anhydrite-rutile-pyrite. Metal solubility decreased gradually with decreasing pressure at all temperatures for both low S and sulfide-saturated models (Fig. 9a-f). The Cu/Au and Cu/Mo ratio decreased over the range 600 to 400 ºC in the low S model, but the Cu/Au ratio at 300 ºC increased with decreasing pressure exceeding that at 400 ºC for pressures below 35 bar; the Cu/Mo ratio at 300 ºC exceeded that at 600 ºC for pressures below ~50 bar (Fig. 9g, i). At sulfide-saturated conditions, the Cu/Au ratio decreased with decreasing temperature by 4 – 5 orders of magnitude (Fig. 9h-j). In contrast, the Cu/Mo ratios increased by 3 – 4 orders of magnitude in the isothermal decompression models performed at lower temperature.

The orders of magnitude decreases in metal solubility predicted by the decompression models described above are analogous to those observed in going from the porphyry to the volcanic gas environment (Fig. 4). The metal contents measured in porphyry-hosted fluid inclusions increase with both temperature and pressure, whereas in the low-pressure volcanic gas environment they vary only slightly as a function of temperature (Fig. 4).

Hurtig, N. C., Migdisov, A. A., and Williams-Jones, A. E., 2021,
••Are Vapor-Like Fluids Viable Ore Fluids for Cu-Au-Mo Porphyry Ore Formation?
Economic Geology, v. 116, p. 1599-1624.

504

505 5.3 Isochoric Cooling

506 Isochoric cooling models combine cooling and decompression and were performed at constant
507 density and the fluid was saturated with ore minerals. Vapor-like intermediate-density fluids (300
508 kg/m^3) and lower-density (100 kg/m^3) vapors were cooled from 600 to 180 ºC at constant density
509 above the critical point of water and along the liquid-vapor curve below the critical point of water
510 (Fig. 4h, Electronic Appendix A). The models only follow the vapor-path below the critical point
511 of water and vapor-liquid partitioning is not considered. The isochoric cooling models were
512 performed for concentrations of 0.1 wt.% and 5.5 wt.% S at 500 ppm Cl and 2.0 wt.% C. The low
513 S models were buffered by magnetite-anhydrite-rutile at high temperature and below 530 ºC by
514 hematite-anhydrite-rutile, whereas the sulfide-saturated models were buffered by anhydrite-rutile-
515 pyrite between 600 and 180 ºC. The R_H traces follow a similar path for both S contents as shown
516 by the representative R_H trace for isochoric cooling models in Figure 5b (Electronic Appendix B).

517 Copper, Mo and Ag solubility decreased with decreasing temperature, whereas Au reached a
518 maximum solubility of 95 ppb – 2.6 ppm between 330 and 510 ºC depending on the density and S
519 content of the vapor (Fig. 10a-d). The Au solubility maximum is more pronounced in the low S
520 models at 500 ppm Cl, for which the dominant species is hydrated AuCl species. At sulfide-
521 saturated conditions, the AuS species is dominant for a Cl concentration of 500 ppm. At higher Cl
522 content (>0.4 wt.% see Fig. 6e), the hydrated AuCl species would be dominant even at sulfide-
523 saturated conditions. As expected from the Au solubility profiles, the Cu/Au ratios reached a
524 minimum at ~300 ºC (Fig. 10e, f). At sulfide-saturated conditions, the Cu/Au ratios decreased
525 continuously during isochoric cooling (Fig. 10g, h) and the Cu/Mo ratio exceeded the Cu/Au ratio.

The effect of fluid density (i.e., the P-T pathway) on metal ratios in the sulfide-saturated model is much less pronounced than in the low S models buffered by magnetite-anhydrite-rutile.

5.4 Mineral Precipitation Models

The deposition of ore minerals (electrum, acanthite, molybdenite, chalcopyrite and bornite) during isochoric cooling of a vapor-like intermediate-density (300 kg/m^3) fluid was evaluated for a range of redox conditions, HCl/$\sum$Cl ratios, S and Cl contents. The P-T path is that of the isochoric cooling model at 300 kg/m^3. Initially, the fluids were undersaturated with respect to ore-forming minerals and then became saturated upon cooling and decompression, triggering ore deposition (Table 4). The metal ratios are based on the S, Cl and redox titration models. The degree of initial ore mineral undersaturation was similar in all precipitation models, except for models presented in Figure 11g and h, in which the excess Cl was increased at constant metal content (that of Fig. 11f). The starting fluid compositions are summarized in Table 4 and are within the range of metal contents reported for natural fluid inclusions (Table 3). Fluid and mineral compositions for all mineral precipitation models are given in the Electronic Appendix B.

We tested a range of starting fluid compositions that fall within the compositional range of a typical porphyry ore fluid (Fig. 11 a-c, e-f). The first set of models was performed for 500 ppm Cl and variable S contents; the redox conditions were buffered by magnetite-anhydrite-rutile (Fig. 11 a-c). These models are specifically designed to evaluate the competition for Cl and S ligands in Au complexation and the effect of S on electrum fineness, Cu/Au and Cu/Mo ratios. The R_H traces for these models vary depending on the S content in the fluid and starting redox buffering assemblage (Fig. 5b). The S-rich model follows a more reduced R_H-pathway compared to the low S model, constraining metal precipitation to higher P-T conditions. At low S content (0.5 wt. %;

Hurtig, N. C., Migdisov, A. A., and Williams-Jones, A. E., 2021,
••Are Vapor-Like Fluids Viable Ore Fluids for Cu-Au-Mo Porphyry Ore Formation?
Economic Geology, v. 116, p. 1599-1624.

starting fluid 0.09 ppm Au), Mo precipitated first at ~ 570 ºC followed by bornite and acanthite at 560 – 480 ºC, chalcopyrite at 510 – 430 ºC, and electrum at ~ 390 ºC (X_{Au} = 0.73 – 0.69; Fig. 11a). At higher S content (1 wt.%; starting fluid 0.14 ppm Au), the amount of precipitated molybdenite was ~5 times lower than in the low S model and the chalcopyrite and electrum zones moved to higher temperatures (550 – 450 ºC and ~400 ºC; Fig. 11b). Slightly more electrum with similar Au-content (X_{Au} = 0.73 – 0.69) precipitated in this model compared to the low S model. At even higher S content (3 wt.% S; 0.74 and 0.47 ppm Au in starting fluids, respectively), the high temperature fluid was either buffered by the assemblage anhydrite-magnetite-rutile (R_H = -3.6 to -4.1, common in porphyry deposits) or a reduced assemblage of anhydrite-magnetite-ilmenite-pyrrhotite (R_H = -2.6 to -3.6, 'reduced' porphyry deposits). In these models, the amount of Au precipitated exceeded that of Mo and the Cu/Au ratios were remarkably low (79 and 248, respectively). In the high S model buffered by anhydrite-magnetite-rutile (R_H = -3.8), Ag and minor Mo deposited at high temperature (~560 ºC); the bulk of the chalcopyrite precipitated at 500 – 400 ºC (Fig. 11c). Electrum precipitated between 560 and 360 ºC and its Au content decreased (0.95 – 0.74) with decreasing temperature and pressure. In the reduced high S model (R_H = -3.2), Cu precipitation was dominated by chalcopyrite, which deposited at higher temperature (580 – 460 ºC) than in the more oxidized high S model, overlapping with Ag and Au mineralization (Fig. 11d). The Au content of the electrum was lower (X_{Au} = 0.89-0.50) and reached a minimum mole fraction of 0.5 at 360 ºC.

The second set of models was performed for 0.3 wt.% Cl and two different S contents to establish a baseline for comparison with models at lower Cl content (Fig. 11e, f) and variable excess Cl i.e., HCl/∑Cl ratio (Fig. 11g, h). The low S model for 0.3 wt.% Cl produced the highest proportion of precipitated Cu-minerals, which was expected as the starting fluid contains 2620

Hurtig, N. C., Migdisov, A. A., and Williams-Jones, A. E., 2021,
••Are Vapor-Like Fluids Viable Ore Fluids for Cu-Au-Mo Porphyry Ore Formation?
Economic Geology, v. 116, p. 1599-1624.

ppm Cu (Table 4; Electronic Appendix B). Increasing the S content at 0.3 wt.% Cl (starting fluid 655 ppm Cu) has a similar effect on metal ratios and the distribution of ore shells to simulations with lower Cl contents (starting fluids 65 – 400 ppm Cu). It is noteworthy that the occurrence of molybdenite and bornite is restricted to the low S models (Fig. 11e, f). In the high Cl models, the precipitation of gold is controlled by the Cl complex and thus increasing the S content has a minimal effect on the amount of electrum precipitated. Models for 1 and 10 wt.% Cl (Fig. 11g, h) were performed for the same metal contents as in the model for 0.3 wt.% Cl (i.e., 655 ppm Cu, 7 ppm Ag, 0.18 ppm Au and 6 ppm Mo). Consequently, the HCl/∑Cl ratio, which represents the proportion of excess Cl to complexed Cl (0 = all Cl is complexed; 1 = all Cl is excess HCl), is higher in simulations with high Cl content. Generally, but not exclusively, volcanic gases and vapor inclusions have the highest HCl/∑Cl ratios (0.7 – 0.99), whereas high T intermediate-density fluid inclusions have moderate ratios (0.3 – 0.7) and brines have the lowest ratios (0.03 – 0.3). For comparison, the HCl/∑Cl ratio was determined to vary between 0.07 and 0.68 in the aqueous phase of experiments involving equilibrium between a silicate melt and an aqueous fluid (Williams et al., 1997).

Lastly, the third set of models tests the sensitivity of ore mineral precipitation as a function of Au, Ag and Cu undersaturation by increasing the Cl content from 0.3 wt.% (Fig. 11f) to 1 and 10 wt.% (Fig. 11g, h). At a Cl content of 1.1 wt.% and a HCl/∑Cl ratio of 0.93, the Cu, Ag and Au ore shells form at lower P-T conditions compared to the model for 0.3 wt.% Cl and 0.76 HCl/∑Cl. For the same starting metal contents, the sequence of metal zoning did not change with increasing Cl content, i.e., degree of Au, Ag and Cu undersaturation. The molybdenum solubility (7 ppm in the starting fluid) is controlled by the $MoO_3(H_2O)_y$ species, thus it is not affected by increasing the amount of Cl in this model and formed its ore shell at similar P-T conditions. At an even higher

Hurtig, N. C., Migdisov, A. A., and Williams-Jones, A. E., 2021,
••Are Vapor-Like Fluids Viable Ore Fluids for Cu-Au-Mo Porphyry Ore Formation?
Economic Geology, v. 116, p. 1599-1624.

595 Cl content of 10 wt.% (0.99 HCl/∑Cl), the Cu and Au ore zones form below the critical point of
596 water (Fig. 11h). At these conditions, the gaseous hydrated silver species (~ 7 ppm Ag) remain
597 stable in the vapor-like fluid leading to the highest electrum fineness. The Mo content decreased
598 to 0.09 ppm in the starting fluid due to the increased stability of solid molybdenum-oxy-chloride
599 limiting the solubility of Mo.
600
601 6. Discussion
602 6.1 Comparison between metal contents and ratios of simulated and natural fluids in porphyry
603 deposits
604 To evaluate the importance of vapor-like fluids for porphyry ore formation, we compare the
605 simulated metal solubility and metal ratios to metal contents measured in vapor-like and
606 intermediate-density fluid inclusions (Fig. 4) and metal ratios of ores in porphyry deposits (Fig.
607 12). The simulated metal solubility and metal ratios change as a function of the fluid composition
608 at 600 ºC and 810 bar i.e., a density of 300 kg/m^3 (Table 5; Figs. 6-8), isothermal decompression
609 (Fig. 9) and isochoric cooling (Fig. 10). We evaluated the metal solubility for R_H values ranging
610 between -4.6 to -1.5. Importantly, we consider simulations buffered by the assemblage magnetite-
611 anhydrite-rutile to be representative of the deep barren stockwork zone in porphyry ore deposits
612 (Fig. 1a; Macdonald and Arnold, 1994; Audétat et al., 2004; Reed et al., 2013) and simulations
613 buffered by pyrite-anhydrite-rutile(-magnetite) to be representative of sulfide-saturated silicate
614 melts in porphyry ore deposits (Halter et al., 2002; Halter et al., 2005; Wilkinson, 2013; Richards,
615 2014; Rottier et al., 2019).
616 At elevated Cl contents (>700 ppm) and high temperature, the solvated Cu species
617 $CuCl(HCl)(H_2O)_y$ is dominant; at lower temperature (<400 °C) the $CuCl(H_2O)_y$ species will

Hurtig, N. C., Migdisov, A. A., and Williams-Jones, A. E., 2021,
••Are Vapor-Like Fluids Viable Ore Fluids for Cu-Au-Mo Porphyry Ore Formation?
Economic Geology, v. 116, p. 1599-1624.

become dominant. The high temperature species comprises of two Cl molecules, resulting in a stronger positive correlation of Cu solubility with increasing Cl content compared to other species containing a single Cl atom i.e., $AuCl(H_2O)_y$ and $AgCl(H_2O)_y$. The potential role of Cu-S species could not be simulated, because the required thermodynamic data were not available. A recent *in-situ* X-ray absorption (XAS) and Raman spectroscopic study (Louvel et al., 2017) designed to investigate the effect of S on Cu transport in water vapor, failed to detect the presence of Cu-S complexes at temperatures between 300 and 600 °C. We therefore conclude that such species are not relevant for the simulated fluid compositions in this study.

The highest Cu (7533 – 8817 ppm) solubility was predicted for fluids in which the Cl content was highest (Fig. 6; Table 5). For comparison, in Reed et al. (2013) copper concentrations ranged from 10 – 6000 ppm in simulations using the HKF-model for liquid-like fluids assuming a starting fluid composition of 8 wt.% S, 2 wt.% Cl (~4 wt.% $NaCl_{eq}$) and 3 wt.% C. Copper concentrations in vapor-like and intermediate-density fluid inclusions range from 10 ppm to 3.3 wt.%, however the highest Cu values were shown to be affected by post-entrapment Cu diffusion into quartz-hosted fluid inclusion (Lerchbaumer and Audétat, 2012). Subsequently, Cu was also measured in topaz- and garnet-hosted vapor inclusions showing concentrations of 56 – 160 ppm (Seo and Heinrich, 2013). For constraining the Cu contents in natural fluid inclusions to realistic values we used PT-C_{Cu} correlations and removed elevated Cu values that did not follow the systematic PT trends (Electronic Appendix B). Here, we suggest that 10 – 4300 ppm Cu with a median of 850 ppm is realistic for vapor-like porphyry fluids based on fluid inclusion data (Table 3). The redox titration models provide a comparable range of 163 – 2785 ppm Cu for vapor-like fluids buffered by magnetite-anhydrite-rutile. In volcanic gas condensates, Cu contents range from 3 ppb to 60 ppm and show a median of 0.3 ppm, which makes Cu the most abundant metal compared to Au,

Hurtig, N. C., Migdisov, A. A., and Williams-Jones, A. E., 2021,
••Are Vapor-Like Fluids Viable Ore Fluids for Cu-Au-Mo Porphyry Ore Formation?
Economic Geology, v. 116, p. 1599-1624.

Ag and Mo in very low-density vapors (Table 3). Copper solubility at the lowest pressure (~8 bar) from decompression models range from 0.07 – 2.5 ppm at 600 °C, 0.08 -1.9 ppb at 400 °C and 0.22 – 21 ppb at 300 °C.

Silver is transported as $AgCl(H_2O)_y$ in vapor-like fluids and is predicted to dissolve in concentrations up to 22 ppm for a Cl concentration of 1 wt.%. This Ag solubility is an order of magnitude lower than that reported in Hurtig and Williams-Jones (2015) for the same Cl concentrations and reflects the strong competition for the chloride ion by Cu species, which were not considered in the earlier study. By comparison, vapor-like and intermediate-density fluid inclusions have been reported to contain up to 190 ppm Ag with a median of 23 ppm (Table 3; Fig. 4g). The lower Ag contents predicted by our current model could reflect the presence of a high temperature gaseous AgS species as suggested by the experiments of Yin and Zajacz (2018), which showed that the Ag concentration in vapor-like hydrothermal fluids increase with increasing H_2S concentration. In the absence of thermodynamic data for gaseous solvated AgS species, however, we were unable to evaluate the potential contribution of AgS species to the transport of Ag in vapor-like fluids. Decompression models at 600 °C predict 0.7 - 3.5 ppb Ag at the lowest pressure (~ 8 bar); at lower temperatures and ~8 bar, Ag values are generally below 1 ppb. Comparatively, the Ag contents for volcanic gases are 3 – 14 ppb, however only 12 of the 136 measurements in our compilation showed detectable Ag contents, indicating that Ag values are likely lower than the limit of detection.

Molybdenum, which dissolves as $MoO_3(H_2O)_y$, had its highest solubility of 230 ppm Mo in oxidizing low S (0.1 wt.%) fluids buffered by magnetite-anhydrite-rutile. Molybdenum solubility correlates positively with increasing f_{O2} (i.e., degreasing R_H) and negatively correlates with S due to the formation of molybdenite (MoS_2), the main Mo ore-forming mineral. Vapor-like and

Hurtig, N. C., Migdisov, A. A., and Williams-Jones, A. E., 2021,
••Are Vapor-Like Fluids Viable Ore Fluids for Cu-Au-Mo Porphyry Ore Formation?
Economic Geology, v. 116, p. 1599-1624.

intermediate-density fluid inclusions in porphyry ore deposits have comparable Mo contents of 1.2 – 290 ppm with a median of 50 ppm (Fig. 4a, b). Some systems, notably Rito del Medio (Zajacz et al., 2008; Audétat, 2019) and Cave Peak (Audétat, 2010) report consistently higher Mo concentrations, than those predicted (80 – 230 ppm) for simulations at 0.1 wt.% S buffered by magnetite-anhydrite-rutile. This could be because NaCl-bearing fluid inclusions in these deposits are of higher density (~350 – 500 kg/m^3) than the density considered in our models (300 kg/m^3). These higher density fluids also have a higher salinity, which could promote the formation of molybdenum oxy-chloride species (Rempel et al., 2008; Ulrich and Mavrogenes, 2008; Borg et al., 2012) or $H_{(2-x)}Na_xMoO_4$ species (Cao, 1989; Kudrin, 1989; Shang et al., 2020) that were not considered in our simulations. Several studies have evaluated the solubility of MoS_2 in hydrothermal liquid-like fluids, however with the exception of Zhang et al. (2012), these studies attributed Mo transport to molybdate or molybdenum oxy-chloride (Wood et al., 1987; Kudrin, 1989) or $HNaMoO_4$ species (Shang et al., 2020). Importantly, Mo shows a strong negative correlation with increasing S content in the experiments of Zhang et al. (2012) and contrary to their interpretation the possibility of Mo-S complexes is unlikely and not predicted by the hard-soft acid-base concept (Pearson, 1963), because Mo(IV) qualifies as a hard metal, which would not easily bond with soft ligands such as reduced sulfur. In decompression models Mo contents range from 4 ppb to 2.5 ppm with increasing temperature (300 – 600 °C) at the lowest pressure (~8 bar) and low S contents and decrease to below 2.4 ppb below 600 °C and high S content (5.5 wt.%). In volcanic gases, the Mo content ranges between 2 ppb and 2.8 ppm Mo (Table 3), which is comparable to the predicted values using the hydration models.

Gold solubility is controlled by hydrated AuCl ($AuCl(H_2O)_y$) and solvated AuS species ($AuS(H_2S)_{x-1}(H_2O)_y$) and thus exhibits a more complex behavior than Cu, Ag or Mo (Figs. 6-8).

Hurtig, N. C., Migdisov, A. A., and Williams-Jones, A. E., 2021,
••Are Vapor-Like Fluids Viable Ore Fluids for Cu-Au-Mo Porphyry Ore Formation?
Economic Geology, v. 116, p. 1599-1624.

687 The highest Au solubility was predicted for models simulated at the highest S content of 10 wt.%.
688 The Au concentrations in these models were 7.6 ppm for a Cl concentration of 500 ppm and 8.2
689 ppm for a Cl concentration of 0.3 wt.%. Gold solubility increased with increasing Cl and S
690 concentrations and a showed a solubility maximum at intermediate redox conditions; the latter is
691 more pronounced for AuS than AuCl. The modeled Au concentrations are comparable to
692 concentrations of 0.05 – 10 ppm Au measured in vapor-like and intermediate-density fluid
693 inclusions (Table 3, Fig. 4e, f). Most vapor-like and intermediate-density fluid inclusions have Au
694 contents below the limit of detection as the compilation consists of only 16 data points. Therefore,
695 accurately predicting Au contents in porphyry ore fluids is challenging and simulations presented
696 in this study provide a new opportunity to investigate reasonable Au contents for vapor-like fluids.
697 Numerical values for simulated Au solubility are given in Table 5 and the Electronic Appendix B
698 for a wide range of conditions. In volcanic gases Au contents range from 7 ppt to 5 ppb (Table 5,
699 Fig. 4e, f). Comparably, simulated Au solubility predicted at 8 bar in decompression models are 9
700 – 73 ppt in the low S models and 0.2 – 16 ppb in the sulfide-saturated models. The highest value
701 of 16 ppb Au was predicted for a fluid comprised of 4.8 wt.% S, 2 wt.% C and 500 ppm Cl at 300
702 °C; at these conditions the AuS species dominates.
703
704 6.2 Fluid evolution pathways: Metal mobility and precipitation
705 Numerical simulations of metal solubility in vapor-like fluids provide a means for evaluating the
706 effects of pressure, temperature and composition on metal solubility and the formation of ore shells
707 in porphyry deposits. Ore mineral precipitation in porphyry deposits is commonly zoned with a
708 high temperature Mo-shell partially overlapped by a telescoped Cu-shell and a narrow shallow Au
709 shell (Fig. 1a; Lowell and Guilbert, 1970; Dilles, 1987; Landtwing et al., 2005; Rusk et al., 2008;

Hurtig, N. C., Migdisov, A. A., and Williams-Jones, A. E., 2021,
••Are Vapor-Like Fluids Viable Ore Fluids for Cu-Au-Mo Porphyry Ore Formation?
Economic Geology, v. 116, p. 1599-1624.

Gruen et al., 2010). However, it is also common that several events of mineralizing fluid produce overlapping ore shells not only in space but also in time (Seedorff and Einaudi, 2004; Gruen et al., 2010).

In Figure 11, we present simulated ore precipitation models that illustrate a single pulse of fluid during isochoric cooling at a density of 300kg/m^3 (see Section 5.3). The Cu/Au (~ 4300) and Cu/Mo ratios (~ 6) predicted by the model with the lowest S content (0.5 wt.%) at 500 ppm Cl are similar to the metal ratios observed in porphyry deposits such as Bingham (Singer et al., 2005). Obviously, the timing of ore formation and subsequent mineralizing pulses are much more complex in natural systems compared to the simplified models presented here. A somewhat lower Cu/Au ratio and higher Cu/Mo ratio is predicted by the model for 1 wt.% S, namely ~2800 and ~30, respectively; these ratios are comparable to those for the Boneng Lobo and Nevados del Famatina porphyry deposits (Singer et al., 2005). In contrast, the predicted Cu/Au and the Cu/Mo ratios for the highest S content (3 wt.%), are ~90 and ~300 at the redox conditions commonly interpreted for porphyry deposits and ~300 and ~8200 for the subset of 'reduced' porphyry deposits (Rowins, 2000; Tarkian et al., 2003), respectively. These ratios are also similar to those observed, for example, in the Dizon and Santo Thomas II porphyry deposits (Singer et al., 2005). These two deposits are not part of the 'reduced' porphyry subclass as they do not contain pyrrhotite and/or ilmenite (Imai, 2001; Imai, 2005). Instead, the presence of high temperature intermediate sulfide solid solutions (iss) and rounded sulfide inclusions (Imai, 2001; Imai, 2005) indicate sulfide-saturated silicate melts in these deposits. As pointed out in the S titration models, the observed Cu/Au and Cu/Mo ratios also depend on the S content of the vapor-like fluid and are indicative of sulfide-saturated systems (>4.8 wt.% S). At high Cl and low S contents (0.3 wt.% Cl, 0.1 wt.% S), the Cu/Au increases to ~ 16'600 and the Cu/Mo ratio is ~30. Increasing the S content

Hurtig, N. C., Migdisov, A. A., and Williams-Jones, A. E., 2021,
••Are Vapor-Like Fluids Viable Ore Fluids for Cu-Au-Mo Porphyry Ore Formation?
Economic Geology, v. 116, p. 1599-1624.

733 to 0.5 wt.% in the high Cl model decreases the Cu/Au ratio to ~3700 and increases the Cu/Mo ratio
734 to 104, showing that the effect of S strongly affects metal ratios also at higher Cl contents.
735 Increasing the HCl/∑Cl ratio does not affect the Cu/Au and Cu/Mo ratios, because the metal
736 contents were kept constant at the same level as models presented in Figure 11f. However, at the
737 highest Cl content of 10 wt.% solid $MoO_2Cl_{2,s}$ starts buffering the Mo content at high T and thus
738 the Cu/Mo ratio increase to ~7400. In conclusion, this indicates that Au-rich porphyry deposits are
739 favored at reduced redox conditions and high S content, and that the interplay between these S
740 content and redox conditions is an important control on the Cu/Au and Cu/Mo ratios in porphyry
741 ore fluids (Fig. 11a-f). In addition to the compositional controls changing, the P-T pathway of the
742 fluid will also affect the shape and distribution of the ore shells. An important conclusion that can
743 be drawn from the numerical precipitation models (Fig. 11) is that the locations and extent of
744 overlap of the Cu, Mo, Au and Ag ore shells vary with the major fluid chemistry (i.e., S, Cl and
745 redox condition) for similar degrees of ore mineral undersaturation. Compositional parameters (S,
746 Cl content, redox conditions) exercise a particularly important control on metal ratios and the metal
747 transport capacity of magmatic fluids. Thus, magma evolution during cooling and crystallization
748 and continued fluid exsolution (Giggenbach, 1996; Webster, 1997; Webster et al., 2009; Webster
749 and Botcharnikov, 2011) may result in variable metal solubility and metal ratios in vapor-like
750 fluids throughout the life-time of magmatic-hydrothermal systems, not captured by the simplified
751 simulations presented in this study.

752 The depth of fluid exsolution (i.e., the lithostatic pressure) and fluid pressure fluctuations
753 within magmatic-hydrothermal plumes are important features that need to be considered in order
754 to fully understand the metal zoning. Numerical simulations of physical processes in magmatic-
755 hydrothermal plumes indicate that they are self-organizing systems, establishing themselves above

Hurtig, N. C., Migdisov, A. A., and Williams-Jones, A. E., 2021,
••Are Vapor-Like Fluids Viable Ore Fluids for Cu-Au-Mo Porphyry Ore Formation?
Economic Geology, v. 116, p. 1599-1624.

the magmatic heat source with a stable temperature front and fluctuations between hydrostatic and lithostatic pressure regimes (Weis et al., 2012; 2014). Thus, depressurization events occur frequently and consequently have been identified in detailed studies investigating vein distribution and vein density in stockwork zones (Gruen et al., 2010). As the stability of hydrated gaseous metal species is highly dependent on pressure and temperature, understanding their behavior in evolving magmatic-hydrothermal systems is a prerequisite for predicting the formation of ore shells and the metal endowment of porphyry deposits. The isothermal decompression models at 600, 400 and 300 ºC show that the solubility of Mo, Ag and Au is strongly dependent on pressure at high temperature (600 ºC) and that this solubility decreases by ~3 – 4 orders of magnitude as pressure decreases from 800 to 10 bar. In contrast, the Cu solubility remains constant for a wide range of pressure (800 to 100 bar) but decreases by ~2 orders of magnitude below ~100 bar (100 to 10 bar). The behavior of hydrated Cu, Au, Ag and Mo species with pressure depends on the number of water molecules in the hydrated species and their stability at elevated temperature; species with high hydration numbers are more sensitive to pressure changes. In natural systems, the concentration of Mo correlates strongly with pressure (Fig. 4b), as is the case for Cu concentrations below ~1500 ppm (Fig. 4d). In contrast, Au concentrations do not display a clear positive correlation with pressure and may also reach a solubility maximum (Fig. 4f). The higher metal concentrations of fluids entrapped at elevated pressures (100 – 1600 bar) compared to those of volcanic gases at atmospheric pressure (~1 bar) are predicted by pressure-dependent simulations at high temperature (600 °C; Fig. 9a, b). At lower temperature (400 and 300 ºC), the concentrations of all the metals considered in this study decreased by 2 – 3 orders of magnitude as pressure decreased from 300 and 80 bar to 10 bar, respectively (Fig. 9b, e). In the sulfide-saturated model, the Au solubility governed by the AuS species shows the least dependence on pressure and only

Hurtig, N. C., Migdisov, A. A., and Williams-Jones, A. E., 2021,
••Are Vapor-Like Fluids Viable Ore Fluids for Cu-Au-Mo Porphyry Ore Formation?
Economic Geology, v. 116, p. 1599-1624.

779 decreased by ~1 order of magnitude as pressure decreased from 80 – 10 bar at 300 ºC, thereby
780 demonstrating the mobility of Au in S-rich vapors at low pressure and temperature.

781 Comparing results from isothermal decompression and isochoric cooling simulations allows
782 for individual analysis of the effects of pressure (i.e., density) at constant T and temperature at
783 constant density on metal ratios in porphyry ore fluids. The isothermal decompression models
784 show that the Cu/Au ratio varies little with pressure and thus depth at 600 ºC (Fig. 9a, b). By
785 contrast, in the isochoric cooling models, gold solubility reaches a maximum between 340 and 510
786 ºC, depending on the fluid density and S content (Fig. 10). These models show that there is a
787 considerable potential for Au re-mobilization during the cooling of magmatic-hydrothermal
788 systems. In the sulfide-saturated simulations, the Au solubility even exceeds that of Cu at low Cl
789 content and a temperature below 300 ºC. This could be potentially important for the formation of
790 anomalous Au-rich porphyry deposits at very shallow depth, such as in the Maricunga Belt (Vila
791 and Sillitoe, 1991; Muntean and Einaudi, 2000; Muntean and Einaudi, 2001) and transport of Au
792 to epithermal environments (Heinrich et al., 2004).
793
794 6.3 Simulated metal ratio trends compared to ore metal ratios in porphyry deposits
795 The predictive power of the numerical simulations and their applicability to natural systems is
796 illustrated in Figure 12. In this figure, we compare the simulated metal ratio evolution paths for
797 titration (Section 5.1), isothermal decompression (Section 5.2) and isochoric cooling (Section 5.3)
798 to metal ratios trends for porphyry deposits (Singer et al., 2005; Fig. 12a). The simulated metal
799 ratios are controlled by ore mineral solubility and thus are considered representative of the relative
800 capacity of the magmatic-hydrothermal plume to transport and precipitate metals in a porphyry
801 setting. These models do not consider potential vapor-melt metal partitioning or the degree of

Hurtig, N. C., Migdisov, A. A., and Williams-Jones, A. E., 2021,
••Are Vapor-Like Fluids Viable Ore Fluids for Cu-Au-Mo Porphyry Ore Formation?
Economic Geology, v. 116, p. 1599-1624.

802 undersaturation of ore forming constituents in magmatic vapors, which have been shown to be
803 important in controlling metal ratios of porphyry ore fluids (Richards, 2013; Wilkinson, 2013).
804 The trends for Cl- and redox-titration, isothermal decompression, and isochoric cooling (Fig.
805 12b) fail to predict the general trend of ore metal ratios in porphyry deposits, which follow a
806 vertical trend at high Mo/Ag ratios with decreasing Cu/Au and a horizontal trend at low Cu/Au
807 ratios with decreasing Mo/Ag ratios (Fig. 12a). Trends for isothermal decompression show an
808 increase in Cu/Au ratios at 600 °C with decreasing pressure between 810 and 20 bar, whereas
809 trends for isochoric cooling show decreasing Cu/Au ratios between 600 °C and 810 bar and 280
810 °C and 64 bar. The Cu/Au ratio in porphyry ore deposits has been shown to decrease with
811 decreasing pressure (Murakami et al., 2010). In this study, we show that isothermal decompression
812 at high T is not responsible for decreasing Cu/Au ratios. However, the Au solubility maximum
813 during isochoric cooling exercises an important control on the Cu/Au ratio and promotes Au
814 mobility at lower temperature and pressure, i.e., in shallow porphyry systems. The behavior of Cu
815 and Au in vapor-like fluids is governed by the interaction of gaseous metal molecules with water
816 molecules (Section 2).
817 It is quite remarkable that the predicted metal ratio evolutionary paths for S-titration models
818 broadly follow the ore metal ratios of porphyry deposits along a vertical trend between 0 – 1 wt.%
819 S and a horizontal trend between 1 – 10 wt.% S (Fig. 12c). The kinks in the vertical part of the
820 model represent variations in the buffering mineral assemblages controlling the redox potential
821 and metal solubility, which mainly affects the Mo/Ag ratio (Section 5.1). Increasing the Cl
822 concentration displaces the modeled S simulation path to a higher Cu/Au ratio. The S-titration
823 models might thus provide an explanation for why some of these deposits (e.g., Bethlehem,

Hurtig, N. C., Migdisov, A. A., and Williams-Jones, A. E., 2021,
••Are Vapor-Like Fluids Viable Ore Fluids for Cu-Au-Mo Porphyry Ore Formation?
Economic Geology, v. 116, p. 1599-1624.

Chuquicamata) have high Cu/Au and Mo/Ag ratios, whereas others (e.g., Grasberg, Galore Creek) have relatively low Cu/Au and Mo/Ag ratios.

Ultimately, the composition of the exsolved magmatic fluid depends on the composition of the magma and the aqueous fluid-melt element partition coefficients. However, the relative solubility of metals in vapor-like fluids controls their transport and precipitation and thus the formation of ore shells. For example, the high S models (> 4.8 wt.%) are representative of sulfide-saturated conditions, at which iss and mss are stable. The presence of magmatic sulfides has been linked to variable sequestration of Cu and Au affecting the Cu/Au ratio of silicate melts during magma evolution and under conditions where iss act as temporary sinks for Au (i.e., releasing it into the ore-forming fluid upon fluid exsolution) it has been argued that the formation of Au-rich porphyry deposits is favored (Halter et al., 2002; 2005; Nadeau et al., 2010; Wilkinson, 2013; Richards, 2014; Nadeau et al., 2016; Rottier et al., 2019). By extension, the high S contents in vapor-like fluids are likely the result of higher S contents in the magma or even the presence of immiscible sulfide melt. Thus, it is reasonable to argue that the positive feedback from an elevated S content in the magma and the vapor-like fluid on the Cu/Au ratio results in the observed trends seen in Figure 12.

Finally, we emphasize that these models need to be refined to accurately predict the metal endowment/ratios for individual deposits by also considering the effects of T, P and redox conditions as well as the Cl and S contents in the fluid and potential undersaturation by considering vapor-melt metal partitioning data and the potential presence of magmatic sulfides.

6.4 Limitations of the numerical simulations

Hurtig, N. C., Migdisov, A. A., and Williams-Jones, A. E., 2021,
••Are Vapor-Like Fluids Viable Ore Fluids for Cu-Au-Mo Porphyry Ore Formation?
Economic Geology, v. 116, p. 1599-1624.

There are several limitations to the numerical simulation approach employed in this study. Firstly, all gases, except H_2O_g, are treated to be ideal. This limitation is a result of introducing thermodynamic properties of gaseous metal species in the form of temperature-dependent logarithmic equilibrium constants of hydration reactions. The fugacity of major gas species is calculated manually after mineral-gas equilibrium calculations have been performed using fugacity coefficients where necessary. Gaseous metal species are linked to water fugacity, i.e., non-ideal behavior of water, by employing a set of hydration reactions for implementation of thermodynamic properties into GEM-Selektor (Electronic Appendix A). Thus, simulations had to be performed at water fugacity and not at total pressure for correct consideration of experimentally fitted thermodynamic properties of gaseous metal species (see Electronic Appendix A for further detail). Partial pressures of major gases such as SO_2, H_2S, CO_2 and HCl, do not exceed ~5 mol% and are less than 2 mol% in most simulations, thus their effect on the total pressure/water fugacity was assumed to be negligible. Secondly, the vapor density is limited to that of pure water, whereas magmatic-hydrothermal fluids are commonly NaCl-bearing with a higher density than that of pure water. This limitation restricted P-T path to the water vapor saturation point and the critical density of pure water. Intermediate-density fluids in the NaCl-H_2O system of 'critical behavior' (homogenization by meniscus disappearance) often have a higher density than can be modeled in the pure water system, which is limited to 322 kg/m^3.

Finally, below the critical point of water the simulations in this study only follow the vapor path and vapor-liquid metal partitioning was not considered. The potential contribution of liquids (i.e., hypersaline brines) to the metal budget was neglected. Therefore, simulated metal solubility below the critical point of water represents minimum metal mobility and ore mineral precipitation is maximized. In porphyry ore-forming systems, however, hypersaline brines are typically present,

Hurtig, N. C., Migdisov, A. A., and Williams-Jones, A. E., 2021,
••Are Vapor-Like Fluids Viable Ore Fluids for Cu-Au-Mo Porphyry Ore Formation?
Economic Geology, v. 116, p. 1599-1624.

and commonly have high metal concentrations (Lerchbaumer and Audétat, 2012; Seo et al., 2012). They could therefore play an important and even dominant role in metal transport after phase separation. Whether hypersaline brines contribute significantly to the metal budget depends on the mole fraction of vapor to liquid in the two-phase mixture (Fig. 1b), the relative mobility of the hypersaline liquid in the magmatic-hydrothermal plumes (Weis et al., 2012; Weis, 2015; Afanasyev et al., 2018) and the efficiency of cooling and ore mineral precipitation from the liquid. As magmatic-hydrothermal plumes vary considerably in their P-T paths(Heinrich, 2005; Williams-Jones and Heinrich, 2005; Driesner and Heinrich, 2007; Audétat, 2019), it follows that there are systems, which will be liquid-dominated and those of the type represented by our simulations, that will be vapor-dominated.

7. Conclusions

Numerical simulations based on metal solubility experiments in vapors provide important insights into the participation of compressible fluids in the formation of magmatic-hydrothermal Cu-Au-Mo-(Ag) deposits. These simulations represent an independent test of the validity of the hypothesis that vapor-like magmatic-hydrothermal fluids carry sufficient Au, Cu, Ag and Mo to be viable ore-forming fluids. This idea has recently been challenged through experimental studies showing that Cu and Au may diffuse in and out of quartz-hosted fluid inclusions, thus questioning the reliability of LA-ICP-MS data obtained from natural vapor-rich fluid (Lerchbaumer and Audétat, 2012).

A key finding of this study was that metal mobility in vapor-like fluids depends strongly on pressure and temperature. As a result, vapor-like fluids can easily deposit large amounts of metals without undergoing phase separation upon decompression thereby connecting low metal contents found in volcanic gases at the surface to orders of magnitude higher metal contents found in fluid

Hurtig, N. C., Migdisov, A. A., and Williams-Jones, A. E., 2021,
••Are Vapor-Like Fluids Viable Ore Fluids for Cu-Au-Mo Porphyry Ore Formation?
Economic Geology, v. 116, p. 1599-1624.

892 inclusions at depth. This observation is critical when considering the efficiency of mineral
893 precipitation from vapor-like fluids compared to that of brines, where cooling and/or fluid-rock
894 reaction would be the driving mechanisms for mineral precipitation. The S content of the fluid was
895 found to exert an important control on metal solubility and metal ratios in vapor-like fluids, which
896 in turn may control the metal endowments and metal ratios in porphyry ore deposits. The major
897 element composition of the vapor-like fluids (SO_2, H_2S, HCl, CO_2) provide the link between
898 aqueous fluids and silicate melts, thus the observed trends may be extended to include melt-vapor
899 processes.

900 The fact that gold solubility reaches a maximum at 340 – 510 ºC, whereas this is not the case
901 for the other gaseous metallic species considered in this study, argues strongly for the hypothesis
902 that Au is preferentially remobilized to shallow, cooler environments such as those of epithermal
903 systems (Heinrich et al., 2004; Williams-Jones and Heinrich, 2005; Henley and Berger, 2011;
904 Hurtig and Williams-Jones, 2015). The Au solubility maximum was also identified as a likely key
905 control on decreasing Cu/Au in shallow porphyry deposits (Murakami et al., 2010).

906 Our numerical simulations have shown that the P-T distribution of ore shells in porphyry ore
907 deposits are controlled by the fluid composition and the P-T paths of the cooling ascending fluids.
908 Recognition of these systematic controls on metal ratios and the formation of ore shells is a
909 discovery that could lead to new strategies for the exploration of porphyry and related ore deposits.
910

911 Acknowledgements

912 Alexander Gysi and Dmitrii Kulik are thanked for their help with implementing experimental
913 data to the GEM-Selektor code package and discussion of numerical simulations. We are grateful
914 for the constructive comments by associate editor Andreas Audétat and reviewers Thomas

Wagner and Christoph Heinrich, that helped improve this manuscript. The funding for this research was provided in part by a NSERC Discovery Grant to AEW-J.

8. References

Afanasyev, A., Blundy, J., Melnik, O., and Sparks, S., 2018, Formation of magmatic brine lenses via focussed fluid-flow beneath volcanoes: Earth and Planetary Science Letters, v. 486, p. 119–128.

Akinfiev, N. N., and Diamond, L. W., 2004, A three-parameter EoS to describe aqueous non-electrolytes at infinite dilution over a wide range of state parameters, with preliminary application to 1:1 electrolytes: Fluid Phase Equilibria, v. 222–223, p. 31–37.

Akinfiev, N. N., and Zotov, A. V., 2016, Solubility of chlorargyrite (AgCl(cr./l.)) in water: New experimental data and a predictive model valid for a wide range of temperatures (273–873K) and water densities (0.01–1g·cm−3): Geochimica et Cosmochimica Acta, v. 178, p. 178–194.

Anderko, A., and Pitzer, K. S., 1993, Equation-of-state representation of phase equilibria and volumetric properties of the system NaCl-H2O above 573 K: Geochimica et Cosmochimica Acta, v. 57, p. 1657–1680.

Anderson, G. M., Castet, S., Schott, J., and Mesmer, R. E., 1991, The density model for estimation of thermodynamic parameters of reactions at high temperatures and pressures: Geochimica et Cosmochimica Acta, v. 55, p. 1769–1779.

Archibald, S. M., Migdisov, A. A., and Williams-Jones, A. E., 2001, The stability of Au-chloride complexes in water vapor at elevated temperatures and pressures: Geochimica et Cosmochimica Acta, v. 65, p. 4413–4423.

938 Archibald, S. M., Migdisov, A. A., and Williams-Jones, Anthony, E., 2002, An experimental
939 study of the stability of copper chloride complexes in water vapor at elevated temperatures
940 and pressures: Geochimica et Cosmochimica Acta, v. 66, p. 1611–1619.
941 Audétat, A., 2010, Source and evolution of molybdenum in the porphyry Mo(-Nb) deposit at
942 Cave Peak, Texas: Journal of Petrology, v. 51, p. 1739–1760.
943 Audétat, A., 2019, The metal content of magmatic-hydrothermal fluids and its relationship to
944 mineralization potential: Economic Geology, v. 114, p. 1033–1056.
945 Audétat, A., Günther, D., and Heinrich, C. A., 2000, Magmatic-hydrothermal evolution in a
946 fractionating granite: A microchemical study of the Sn-W-F-mineralized mole granite
947 (Australia): Geochimica et Cosmochimica Acta, v. 64, p. 3373–3393.
948 Audétat, A., Pettke, T., and Dolejš, D., 2004, Magmatic anhydrite and calcite in the ore-forming
949 quartz-monzodiorite magma at Santa Rita, New Mexico (USA): Genetic constraints on
950 porphyry-Cu mineralization: Lithos, v. 72, p. 147–161.
951 Bischoff, J., Rosenbauer, R., and Pitzer, K., 1986, The system NaCl-H2O: Relations of vapor-
952 liquid near the critical temperature of water and of vapor-liquid-halite from 300° to 500°C:
953 Geochimica et Cosmochimica Acta, v. 50, p. 1437–1444.
954 Bodnar, R. J., and Beane, R. E., 1980, Temporal and Spatial Variations in Hydrothermal Fluid
955 Characterisitics during Vein Filling in Preore Cover Overlying Deeply Buried Porpyry
956 Copper-Type Mineralization at Red Mountain, Arizona: Economic Geology, v. 75, p. 876–
957 893.
958 Borg, S., Liu, W., Etschmann, B., Tian, Y., and Brugger, J., 2012, An XAS study of
959 molybdenum speciation in hydrothermal chloride solutions from 25-385°C and 600 bar:
960 Geochimica et Cosmochimica Acta, v. 92, p. 292–307.

961 Born, M., 1920, Volumes of heats of hydration of ions: Z. Phys., v. 1, p. 45–48.
962 Bucher, M., and Porter, T. L., 1986, Analysis of the born model for hydration of ions: Journal of
963 Physical Chemistry, v. 90, p. 3406–3411.
964 Cao, X., 1989,Solubility of molybdenite and the transport of molybdenum in hydrothermal
965 solutions: Iowa State University: 103 p.
966 Chase, M. W., 1998, NIST-JANAF Thermochemical Tables: J. Phys. Chem. Ref. Data, p. 1–
967 1952.
968 Cooke, D. R., Hollings, P., and Walshe, J. L., 2005, Giant Porphyry Deposits: Characterisitics,
969 Distribution and Tectonic Controls: Economic Geology, v. 100, p. 801–818.
970 Dagade, D. H., and Barge, S. S., 2016, Hydrogen Bonding in Liquid Water and in the Hydration
971 Shell of Salts: ChemPhysChem, v. 17, p. 902–912.
972 Dilles, J. H., 1987, Petrology of the Yerington Batholith, Nevada: Evidence for Evolution of
973 Porphyry Copper Ore Fluids: Economic Geology, v. 82, p. 1750–1789.
974 Driesner, T., and Heinrich, C., 2007, The system H2O–NaCl. Part I: Correlation formulae for
975 phase relations in temperature–pressure–composition space from 0 to 1000°C, 0 to 5000bar,
976 and 0 to 1 XNaCl: Geochimica et Cosmochimica Acta, v. 71, p. 4880–4901.
977 Eastoe, C. J., 1978, A fluid inclusion Study of the Panguna Porphyry Copper Deposit,
978 Bougainville, Papua New Guinea: Economic Geology, v. 73, p. 721–748.
979 Eastoe, C. J., 1982, Physics and chemistry of the hydrothermal system at the Panguna porphyry
980 copper deposit, Bougainville, Papua New Guinea.: Economic Geology, v. 77, p. 127–153.
981 Einaudi, M. T., Hedenquist, J. W., and Inan, E. E., 2003, Sulfidation State of Fluids in Active
982 and Extinct Hydrothermal Systems: Transitions from Porphyry to Epithermal
983 Environments: Soc Econ Geol Spec Publ, v. 10, p. 1–50.

Etschmann, B., Liu, W., Testemale, D., Müller, H., Rae, N. a., Proux, O., Hazemann, J. L., and Brugger, J., 2010, An in situ XAS study of copper(I) transport as hydrosulfide complexes in hydrothermal solutions (25˚C to 600˚C, 180 to 600bar): speciation in vapor and liquid phases: Geochimica et Cosmochimica Acta, v. 74, p. 4723–4739.

Evans, K. A., Powell, R., and Holland, T. J. B., 2010, Internally consistent data for sulphur-bearing phases and application to the construction of pseudosections for mafic greenschist facies rocks in Na2O-CaO-K2O-FeO-MgO-Al2O3-SiO2-CO2-O-S-H2O: Journal of Metamorphic Geology, v. 28, p. 667–687.

Fernández, D. P., Goodwin, a R. H., Lemmon, E. W., Levelt Sengers, J. M. H., and Williams, R. C., 1997, A formulation of the static permittivity of water and steam at temperatures from 283 K to 873 K at pressures up to 1200 MPa, including derivatives and Deby-Hückel coefficients: J. Phys. Chem. Ref. Data, v. 26, p. 1125–1166.

Frank, M. R., Candela, P. A., Piccoli, P. M., and Glascock, M. D., 2002, Gold solubility, speciation, and partitioning as a function of HCl in the brine-silicate melt-metallic gold system at 800°C and 100 MPa: Geochimica et Cosmochimica Acta, v. 66, p. 3719–3732.

Frank, M. R., Candela, P. A., and Piccoli, P. M., 2003, Alkali exchange equilibria between a silicate melt and coexisting magmatic volatile phase: An experimental study at 800°C and 100 MPa: Geochimica et Cosmochimica Acta, v. 67, p. 1415–1427.

Franks, F., 1973, The Solvent Properties of Water, in Water in Crystalline Hydrates Aqueous Solutions of Simple Nonelectrolytes: Springer US, p. 1–54.

Frenkel, M. L., 1994, Thermodynamics of organic compounds in the gas state: CRC press, v. 1.

Gemmell, J. B., 1987, Geochemistry of metallic trace elements in fumarolic condensates from Nicaraguan and Costa Rican volcanoes: Journal of Volcanology and Geothermal Research,

v. 33, p. 161–181.

Giggenbach, W. F., 1981, Geothermal mineral equilibria: Geochimica et Cosmochimica Acta, v. 45, p. 393–410.

Giggenbach, W. F., 1987, Redox processes governing the chemistry of fumarolic gas discharges from White Island, New Zealand: Applied Geochemistry, v. 2, p. 143–161.

Giggenbach, W. F., 1996, Chemical Composition of Volcanic Gases: Monitoring and Mitigation of Volcanic Hazards, p. 221–256.

Giggenbach, W. F., and Matsuo, S., 1991, Evaluation of results from Second and Third IAVCEI Field Workshops on Volcanic Gases, Mt Usu, Japan, and White Island, New Zealand: Applied Geochemistry, v. 6, p. 125–141.

Godinho, S. S. M. C., Cabral do Couto, P., and Costa Cabral, B. J., 2005, Polarization effects and charge separation in AgCl-water clusters.: The Journal of chemical physics, v. 122, p. 44316.

Grønvold, F., and Westrum, E. F., 1986, Silver(I) sulfide: Ag2S Heat capacity from 5 to 1000 K, thermodynamic properties, and transitions: The Journal of Chemical Thermodynamics, v. 18, p. 381–401.

Gruen, G., Heinrich, C. A., and Schroeder, K., 2010, The Bingham Canyon porphyry Cu-Mo-Au deposit. II. Vein geometry and ore shell formation by pressure-driven rock extension: Economic Geology, v. 105, p. 69–90.

Gruen, G., Weis, P., Driesner, T., De Ronde, C. E. J., and Heinrich, C. A., 2012, Fluid-flow patterns at brothers volcano, Southern Kermadec Arc: Insights from geologically constrained numerical simulations: Economic Geology, v. 107, p. 1595–1611.

Gustafson, L. B., and Hunt, J. P., 1975, The porphyry copper deposit at El Salvador, Chile:

Economic Geology, v. 70, p. 857–912.

Halter, W. E., Pettke, T., and Heinrich, C. A., 2002, The origin of Cu/Au ratios in porphyry-type ore deposits: Science, v. 296, p. 1844–1846.

Halter, W. E., Heinrich, C. A., and Pettke, T., 2005, Magma evolution and the formation of porphyry Cu-Au ore fluids: Evidence from silicate and sulfide melt inclusions: Mineralium Deposita, v. 39, p. 845–863.

Hannay, J. B., Hogarth, J., and Stokes, G. G., 1880, On the Solubility of Solids in Gases: Proceedings of the royal society of London, v. 30, p. 178–188.

Hedenquist, J. W., Masahiro, A., and Shinohara, H., 1994, Flux of volatiles and ore-forming metals from the magmatic-hydrothermal system of Satsuma Iwojima volcano: Geology, v. 22, p. 585–588.

Hedenquist, J. W., Arribas, A., and Reynolds, T. J., 1998, Evolution of an intrusion-centered hydrothermal system; Far Southeast-Lepanto porphyry and epithermal Cu-Au deposits, Philippines: Economic Geology, v. 93, p. 373–404.

Heinrich, C. A., 2005, The physical and chemical evolution of low-salinity magmatic fluids at the porphyry to epithermal transition: A thermodynamic study: Mineralium Deposita, v. 39, p. 864–889.

Heinrich, C. A., Günther, D., Audétat, A., Ulrich, T., and Frischknecht, R., 1999, Metal fractionation between magmatic brine and vapor, determined by microanalysis of fluid inclusions: Geology, v. 27, p. 755.

Heinrich, C. A., Driesner, T., Stefánsson, A., and Seward, T. M., 2004, Magmatic vapor contraction and the transport of gold from the porphyry environment to epithermal ore deposits: Geology, v. 32, p. 761.

1053 Helgeson, H. C., Kirkham, D. H., and Flowers, G. C., 1981, Theoretical prediction of the
1054 thermodynamic behavior of aqueous electrolytes at high pressures and temperatures: IV.
1055 Calculation of activity coefficients, osmotic coefficients, and apparent molal and standard
1056 and relative partial molal properties to 600 °: Am. J. Sci., v. 281, p. 1249–1516.
1057 Henley, R. W., and Berger, B. R., 2011, Magmatic-vapor expansion and the formation of high-
1058 sulfidation gold deposits: Chemical controls on alteration and mineralization: Ore Geology
1059 Reviews, v. 39, p. 63–74.
1060 Henley, R. W., and McNabb, A., 1978, Magmatic vapor plumes and ground-water interaction in
1061 porphyry copper emplacement: Economic Geology, v. 73, p. 1–18.
1062 Henley, R. W., and Seward, T. M., 2018, Gas–Solid Reactions in Arc Volcanoes: Ancient and
1063 Modern: Reviews in Mineralogy and Geochemistry, v. 84, p. 309–349.
1064 Hezarkhani, A., and Williams-Jones, A. E., 1998, Controls of Alteration and Mineralization in
1065 the Sungun Porphyry Copper Deposit, Iran: Evidence from Fluid Inclusions and Stable
1066 Isotopes: Economic Geology, v. 93, p. 651–670.
1067 Holland, T., and Powell, R., 1998, An internally consistent thermodynamic data set for phases of
1068 petrological interest: Journal of Metamorphic Geology, v. 16, p. 309–343.
1069 Holland, T. J. B., and Powell, R., 2011, An improved and extended internally consistent
1070 thermodynamic dataset for phases of petrological interest, involving a new equation of state
1071 for solids: Journal of Metamorphic Geology, v. 29, p. 333–383.
1072 Hurtig, N. C., and Williams-Jones, A. E., 2014a, An experimental study of the solubility of
1073 MoO3 in aqueous vapour and low to intermediate density supercritical fluids: Geochimica
1074 et Cosmochimica Acta, v. 136, p. 169–193.
1075 Hurtig, N. C., and Williams-Jones, A. E., 2014b, An experimental study of the transport of gold

through hydration of AuCl in aqueous vapour and vapour-like fluids: Geochimica et Cosmochimica Acta, v. 127, p. 305–325.

Hurtig, N. C., and Williams-Jones, A. E., 2015, Porphyry-epithermal Au-Ag-Mo ore formation by vapor-like fluids: New insights from geochemical modeling: Geology, v. 43, p. 587–590.

Imai, A., 2001, Generation of ore fluids for porphyry copper gold mineralization of the Santo Tomas II (Philex) Deposit, Philippines.: Resource Geology, v. 51, p. 71–96.

Imai, A., 2005, Evolution of Hydrothermal System at the Dizon Porphyry Cu-Au Deposit, Zambales, Philippines: Resource Geology, v. 55, p. 73–90.

Johnson, J. W., Oelkers, E. H., and Helgeson, H. C., 1992, SUPCRT92: A software package for calculating the standard molal thermodynamic properties of minerals, gases, aqueous species, and reactions from 1 to 5000 bar and 0 to 1000 ºC: Computers & Geosciences, v. 18, p. 899–947.

Karpov, I. K., Chudnenko, K. V., Kulik, D. A., and Bychinskii, V. A., 2002, The convex programming minimization of five thermodynamic potentials other than Gibbs energy in geochemical modeling: American Journal of Science, v. 302, p. 281–311.

Karpov, I. K. K., Chudnenko, K. V. V, Kulik, D. A. A., Avchenko, O. V. V, and Bychinski, V. A. A., 2001, Minimization of Gibbs free energy in geochemical systems by convex programming: Geochemistry International, v. 39, p. 1108–1119.

Klemm, L. M., Pettke, T., Heinrich, C. A., and Campos, E., 2007, Hydrothermal evolution of the El Teniente deposit, Chile: Porphyry Cu-Mo ore deposition from low-salinity magmatic fluids: Economic Geology, v. 102, p. 1021–1045.

Klemm, L. M., Pettke, T., and Heinrich, C. A., 2008, Fluid and source magma evolution of the Questa porphyry Mo deposit, New Mexico, USA: Mineralium Deposita, v. 43, p. 533–552.

1099 Koděra, P., Heinrich, C. A., Wälle, M., and Lexa, J., 2014, Magmatic salt melt and vapor:
1100 Extreme fluids forming porphyry gold deposits in shallow subvolcanic settings: Geology, v.
1101 42, p. 495–498.
1102 Krauskopf, K. B., 1957, The heavy metal content of magmatic vapor at 600 degrees C:
1103 Economic Geology, v. 52, p. 786.
1104 Krauskopf, K. B., 1964, The possible role of volatile metal compounds in ore genesis: Economic
1105 Geology, v. 59, p. 22–45.
1106 Kudrin, A. V., 1989, Behavior of Mo in aqueous NaCl and KCl solutions at 300-450°C:
1107 Geochemistry International, v. 26, p. 87–99.
1108 Kulik, D. A., Wagner, T., Dmytrieva, S. V., Kosakowski, G., Hingerl, F. F., Chudnenko, K. V.,
1109 and Berner, U. R., 2013, GEM-Selektor geochemical modeling package: Revised algorithm
1110 and GEMS3K numerical kernel for coupled simulation codes: Computational Geosciences,
1111 v. 17, p. 1–24.
1112 Landtwing, M. R., Pettke, T., Halter, W. E., Heinrich, C. A., Redmond, P. B., Einaudi, M. T.,
1113 and Kunze, K., 2005, Copper deposition during quartz dissolution by cooling magmatic-
1114 hydrothermal fluids: The Bingham porphyry: Earth and Planetary Science Letters, v. 235, p.
1115 229–243.
1116 Landtwing, M. R., Furrer, C., Redmond, P. B., Pettke, T., Guillong, M., and Heinrich, C. a.,
1117 2010, The Bingham Canyon Porphyry Cu-Mo-Au Deposit. III. Zoned Copper-Gold Ore
1118 Deposition by Magmatic Vapor Expansion: Economic Geology, v. 105, p. 91–118.
1119 Lecumberri-Sanchez, P., Steele-MacInnis, M., Weis, P., Driesner, T., and Bodnar, R. J., 2015,
1120 Salt precipitation in magmatic-hydrothermal systems associated with upper crustal plutons:
1121 Geology, v. 43, p. 1063–1066.

1122 Lerchbaumer, L., and Audétat, A., 2012, High Cu concentrations in vapor-type fluid inclusions:
1123 An artifact? Geochimica et Cosmochimica Acta, v. 88, p. 255–274.
1124 Lerchbaumer, L., and Audétat, A., 2013, The metal content of silicate melts and aqueous fluids
1125 in subeconomically mo mineralized granites: Implications for porphyry mo genesis:
1126 Economic Geology, v. 108, p. 987–1013.
1127 Liu, W., Brugger, J., Etschmann, B., Testemale, D., and Hazemann, J., 2008, The solubility of
1128 nantokite (CuCl(s)) and Cu speciation in low-density fluids near the critical isochore: An in-
1129 situ XAS study: Geochimica et Cosmochimica Acta, v. 72, p. 4094–4106.
1130 Louvel, M., Bordage, A., Tripoli, B., Testemale, D., Hazemann, J. L., and Mavrogenes, J., 2017,
1131 Effect of S on the aqueous and gaseous transport of Cu in porphyry and epithermal systems:
1132 Constraints from in situ XAS measurements up to 600 °C and 300 bars: Chemical Geology,
1133 v. 466, p. 500–511.
1134 Lowell, J. D., and Guilbert, J. M., 1970, Lateral and Vertical Alteration-Mineralization Zoning in
1135 Porphyry Ore Deposits: Economic Geology, v. 65, p. 373–408.
1136 Macdonald, G. D., and Arnold, L. C., 1994, Geological and Geochemical Zoning of the Grasberg
1137 Igneous Complex, Irian-Jaya, Indonesia: Journal of Geochemical Exploration, v. 50, p.
1138 143–178.
1139 Majer, V., Sedlbauer, J., and Bergin, G., 2008, Henry's law constant and related coefficients for
1140 aqueous hydrocarbons, CO2 and H2S over a wide range of temperature and pressure: Fluid
1141 Phase Equilibria, v. 272, p. 65–74.
1142 Marshall, W. L., and Franck, E. U., 1981, Ion product of water substance, 0-1000 °C, 1-10,000
1143 bars New International Formulation and its background: Journal of Physical and Chemical
1144 Reference Data, v. 10, p. 295–304.

1145 Mei, Y., Liu, W., Sherman, D. M., and Brugger, J., 2014, Metal complexation and ion hydration
1146 in low density hydrothermal fluids: Ab initio molecular dynamics simulation of Cu(I) and
1147 Au(I) in chloride solutions (25-1000°C, 1-5000bar): Geochimica et Cosmochimica Acta, v.
1148 131, p. 196–212.
1149 Mei, Y., Liu, W., Migdiov, A. A., and Brugger, J., 2018, CuCl Complexation in the Vapor
1150 Phase : Insights from Ab Initio Molecular Dynamics Simulations: Geofluids, p. 1–12.
1151 Mejías, J. A., and Lago, S., 2000, Calculation of the absolute hydration enthalpy and free energy
1152 of H+ and OH-: Journal of Chemical Physics, v. 113, p. 7306–7316.
1153 Mercer, C. N., and Reed, M. H., 2013, Porphyry Cu-Mo stockwork formation by dynamic,
1154 transient hydrothermal pulses: Mineralogic insights from the deposit at Butte, Montana:
1155 Economic Geology, v. 108, p. 1347–1377.
1156 Mernagh, T. P., Leys, C., and Henley, R. W., 2020, Fluid inclusion systematics in porphyry
1157 copper deposits: The super-giant Grasberg deposit, Indonesia, as a case study: Ore Geology
1158 Reviews, v. 123, p. 103570.
1159 Migdisov, A. A., and Williams-Jones, A. E., 2013, A predictive model for metal transport of
1160 silver chloride by aqueous vapor in ore-forming magmatic-hydrothermal systems:
1161 Geochimica et Cosmochimica Acta, v. 104, p. 123–135.
1162 Migdisov, A. A., Williams-Jones, a. E., and Suleimenov, O. M., 1999, Solubility of
1163 chlorargyrite (AgCl) in water vapor at elevated temperatures and pressures: Geochimica et
1164 Cosmochimica Acta, v. 63, p. 3817–3827.
1165 Migdisov, A. A., Bychkov, A. Y., Williams-Jones, A. E., and van Hinsberg, V. J., 2014, A
1166 predictive model for the transport of copper by HCl-bearing water vapour in ore-forming
1167 magmatic-hydrothermal systems: Implications for copper porphyry ore formation:

1168 Geochimica et Cosmochimica Acta, v. 129, p. 33–53.
1169 Monecke, T., Monecke, J., James Reynolds, T., Tsuruoka, S., Bennett, M. M., Skewes, W. B.,
1170 and Palin, R. M., 2018, Quartz solubility in the H2O-NaCl system: A framework for
1171 understanding vein formation in porphyry copper deposits: Economic Geology, v. 113, p.
1172 1007–1046.
1173 Morey, G. W., 1957, The solubility of solids in gases: Economic Geology, v. 52, p. 225–251.
1174 Morey, G. W., and Hesselgesser, J. M., 1951, The solubility of some minerals in superheated
1175 steam at high pressures: Economic Geology, v. 46, p. 821–835.
1176 Muntean, J. L., and Einaudi, M. T., 2000, Porphyry Gold Deposits of the Refugio District,
1177 Maricunga Belt, Northern Chile: Economic Geology, v. 95, p. 1445–1472.
1178 Muntean, J. L., and Einaudi, M. T., 2001, Porphyry-Epithermal Transition: Maricunga Belt,
1179 Northern Chile: Economic Geology, v. 96, p. 743–772.
1180 Murakami, H., Seo, J. H., and Heinrich, C. A., 2010, The relation between Cu/Au ratio and
1181 formation depth of porphyry-style Cu-Au ± Mo deposits: Mineralium Deposita, v. 45, p.
1182 11–21.
1183 Nadeau, O., Williams-Jones, A. E., and Stix, J., 2010, Sulphide magma as a source of metals in
1184 arc-related magmatic hydrothermal ore fluids: Nature Geoscience, v. 3, p. 501–505.
1185 Nadeau, O., Stix, J., and Williams-Jones, A. E., 2016, Links between arc volcanoes and
1186 porphyry-epithermal ore deposits: Geology, v. 44, p. 11–14.
1187 Pitzer, K. S., and Pabalan, R. T., 1986, Thermodynamics of NaCl in steam: Geochimica et
1188 Cosmochimica Acta, v. 50, p. 1445–1454.
1189 Pitzer, K. S., Bischoff, J. L., and Rosenbauer, R. J., 1987, CRITICAL BEHAVIOR OF DILUTE
1190 NaCL IN H2O: Chemical Physics Letters, v. 134, p. 60–63.

1191 Pokrovski, G. S., Roux, J., and Harrichoury, J.-C., 2005, Fluid density control on vapor-liquid
1192 partitioning of metals in hydrothermal systems: Geology, v. 33, p. 657.
1193 Pokrovski, G. S., Borisova, A. Y., and Bychkov, A. Y., 2013, Speciation and Transport of Metals
1194 and Metalloids in Geological Vapors: Reviews in Mineralogy and Geochemistry, v. 76, p.
1195 165–218.
1196 Proffett, J. M., 2009, High Cu grades in porphyry Cu deposits and their relationship to
1197 emplacement depth of magmatic sources: Geology, v. 37, p. 675–678.
1198 Proust, P., and Vera, J. H., 1989, PRSV: The Stryjek-Vera modification of the Peng-Robinson
1199 equation of state. Parameters for other pure compounds of industrial interest: The Canadian
1200 Journal of Chemical Engineering, v. 67, p. 170–173.
1201 Redmond, P. B., and Einaudi, M. T., 2010, The Bingham Canyon porphyry Cu-Mo-Au deposit.
1202 I. Sequence of intrusions, vein formation, and sulfide deposition: Economic Geology, v.
1203 105, p. 43–65.
1204 Redmond, P. B., Einaudi, M. T., Inan, E. E., Landtwing, M. R., and Heinrich, C. A., 2004,
1205 Copper deposition by fluid cooling in intrusion-centered systems: New insights from the
1206 Bingham porphyry ore deposit, Utah: Geology, v. 32, p. 217–220.
1207 Reed, M., Rusk, B., and Palandri, J., 2013, The Butte magmatic-hydrothermal system: One fluid
1208 yields all alteration and veins: Economic Geology, v. 108, p. 1379–1396.
1209 Rempel, K. U., Migdisov, A. A., and Williams-Jones, A. E., 2006, The solubility and speciation
1210 of molybdenum in water vapour at elevated temperatures and pressures: Implications for ore
1211 genesis: Geochimica et Cosmochimica Acta, v. 70, p. 687–696.
1212 Rempel, K. U., Williams-Jones, A. E., and Migdisov, A. A., 2008, The solubility of
1213 molybdenum dioxide and trioxide in HCl-bearing water vapour at 350 °C and pressures up

Hurtig, N. C., Migdisov, A. A., and Williams-Jones, A. E., 2021,
••Are Vapor-Like Fluids Viable Ore Fluids for Cu-Au-Mo Porphyry Ore Formation?
Economic Geology, v. 116, p. 1599-1624.

1214 to 160 bars: Geochimica et Cosmochimica Acta, v. 72, p. 3074–3083.
1215 Richards, J. P., 2013, Giant ore deposits formed by optimal alignments and combinations of
1216 geological processes: Nature Geoscience, v. 6, p. 911–916.
1217 Richards, J. P., 2014, The oxidation state, and sulfur and Cu contents of arc magmas:
1218 Implications for metallogeny: Lithos, v. 233, p. 27–45.
1219 Robie, R. A., and Hemingway, B. S., 1995, Thermodynamic properties of minerals and related
1220 substances at 298.15 K and 1 bar (105 pascals) pressure and at higher temperatures: U. S.
1221 Geological Survey Bulletin, v. 2131, p. 461.
1222 Robie, R. A., Seal, R. R., and Hemingway, B. S., 1994, Heat capacity and entropy of bornite
1223 (Cu5FeS4) between 6 and 760 K and the thermodynamic properties of phases in the system
1224 Cu-Fe-S: Canadian Mineralogist, v. 32, p. 945–956.
1225 Rottier, B., Audétat, A., Koděra, P., and Lexa, J., 2019, Origin and Evolution of Magmas in the
1226 Porphyry Au-mineralized Javorie Volcano (Central Slovakia): Evidence from
1227 Thermobarometry, Melt Inclusions and Sulfide Inclusions: Journal of Petrology, v. 60, p.
1228 2449–2482.
1229 Rowins, S. M., 2000, Reduced porphyry copper-gold deposits: A new variation on an old theme:
1230 Geology, v. 28, p. 491–494.
1231 Rusk, B., and Reed, M., 2002, Scanning electron microscope-cathodoluminescence analysis of
1232 quartz reveals complex growth histories in veins from the Butte porphyry copper deposit,
1233 Montana: Geology, v. 30, p. 727–730.
1234 Rusk, B. G., Reed, M. H., Dilles, J. H., Klemm, L. M., and Heinrich, C. A., 2004, Compositions
1235 of magmatic hydrothermal fluids determined by LA-ICP-MS of fluid inclusions from the
1236 porphyry copper-molybdenum deposit at Butte, MT: Chemical Geology, v. 210, p. 173–

199.

Rusk, B. G., Reed, M. H., and Dilles, J. H., 2008, Fluid Inclusion Evidence for Magmatic-Hydrothermal fluid evolution in the porphyry copper-molybdenum deposit at Butte, Montana: Economic Geology, v. 103, p. 307–334.

Scher, S., Williams-Jones, A. E., and Williams-Jones, G., 2013, Fumarolic activity, acid-sulfate alteration, and high sulfidation epithermal precious metal mineralization in the crater of Kawah Ijen volcano, Java, Indonesia: Economic Geology, v. 108, p. 1099–1118.

Schöpa, A., Annen, C., Dilles, J. H., Sparks, R. S. J., and Blundy, J. D., 2017, Magma emplacement rates and porphyry copper deposits: Thermal modeling of the yerington batholith, Nevada: Economic Geology, v. 112, p. 1653–1672.

Seedorff, E., and Einaudi, M. T., 2004, Henderson Porphyry Molybdenum System, Colorado: II.Decoupling of Introduction and Deposition of Metals during GeochemicalEvolution of Hydrothermal Fluids: Economic Geology, v. 99, p. 39–72.

Seo, J. H., and Heinrich, C. A., 2013, Selective copper diffusion into quartz-hosted vapor inclusions: Evidence from other host minerals, driving forces, and consequences for Cu-Au ore formation: Geochimica et Cosmochimica Acta, v. 113, p. 60–69.

Seo, J. H., Guillong, M., and Heinrich, C. A., 2009, The role of sulfur in the formation of magmatic-hydrothermal copper-gold deposits: Earth and Planetary Science Letters, v. 282, p. 323–328.

Seo, J. H., Guillong, M., Aerts, M., Zajacz, Z., and Heinrich, C. A., 2011, Microanalysis of S, Cl, and Br in fluid inclusions by LA-ICP-MS: Chemical Geology, v. 284, p. 35–44.

Seo, J. H., Guillong, M., and Heinrich, C. A., 2012, Separation of molybdenum and copper in porphyry deposits: The roles of sulfur, redox, and pH in ore mineral deposition at bingham

canyon: Economic Geology, v. 107, p. 333–356.

Shang, L., Williams-Jones, A. E., Wang, X., Timofeev, A., Hu, R., and Bi, X., 2020, An Experimental Study of the Solubility and Speciation of MoO3(s) in Hydrothermal Fluids at Temperatures up to 350°C: Economic Geology, v. 3, p. 1–10.

Sillitoe, R. H., 1973, The tops and bottoms of porphyry copper deposits: Economic Geology, v. 68, p. 799–815.

Sillitoe, R. H., 2010, Porphyry copper systems: Economic Geology, v. 105, p. 3–41.

Simon, A., Pettke, T., Candela, P., Piccoli, P., and Heinrich, C., 2007, The partitioning behavior of As and Au in S-free and S-bearing magmatic assemblages: Geochimica et Cosmochimica Acta, v. 71, p. 1764–1782.

Simon, A. C., Frank, M. R., Pettke, T., Candela, P. A., Piccoli, P. M., and Heinrich, C. A., 2005, Gold partitioning in melt-vapor-brine systems: Geochimica et Cosmochimica Acta, v. 69, p. 3321–3335.

Simon, A. C., Pettke, T., Candela, P. A., Piccoli, P. M., and Heinrich, C. A., 2006, Copper partitioning in a melt-vapor-brine-magnetite-pyrrhotite assemblage: Geochimica et Cosmochimica Acta, v. 70, p. 5583–5600.

Simon, A. C., Pettke, T., Candela, P. A., and Piccoli, P. M., 2008, The partitioning behavior of silver in a vapor-brine-rhyolite melt assemblage: Geochimica et Cosmochimica Acta, v. 72, p. 1638–1659.

Sinclair, W. D., 2007, Porphyry Deposits, in Mineral Deposits of Canada: A synthesis of major deposit-types, districs metallogeny, the evolution of geological provinces and exploration methods: Geological Association of Canada, Mineral Deposits Devision, p. 223–243.

Singer, D. a., Berger, V. I., and Moring, B. C., 2005, Porphyry Copper Deposits of the World

1283 Database, Map, and Grade and Tonnage Models:, accessed at Open-file Report 2005-1060
1284 at http://pubs.usgs.gov/of/2005/1060/.
1285 Stefánsson, A., and Arnórsson, S., 2002, Gas pressures and redox reactions in geothermal fluids
1286 in Iceland: Chemical Geology, v. 190, p. 251–271.
1287 Sterner, S., Chou, I., Downs, R., and Pitzer, K., 1992, Phase relations in the system NaCl-KCl-
1288 H2O: V. Thermodynamic- PTX analysis of solid-liquid equilibria at high temperatures and
1289 pressures: Geochimica et cosmochimica …, v. 56, p. 2295–2309.
1290 Stryjek, R., Vera, J. H., Engineering, C., and Ha, C., 1986, PRSV : An Improved Peng- Robinson
1291 Equation of State for Pure Compounds and Mixtures: The Canadian Journal of Chemical
1292 Engineering, v. 64, p. 323–333.
1293 Symonds, R., Rose, W., Reed, M., Lichte, F., and Finnegan, D., 1987, Volatilization, transport
1294 and sublimation of metallic and non-metallic elements in high temperature gases at Merapi
1295 Volcano, Indonesia: Geochimica et Cosmochimica Acta, v. 51, p. 2083–2101.
1296 Symonds, R. B., Rose, W. I., Gerlach, T. M., Briggs, P. H., and Harmon, R. S., 1990, Evaluation
1297 of gases, condensates, and SO2emissions from Augustine volcano, Alaska: the degassing of
1298 a Cl-rich volcanic system: Bulletin of Volcanology, v. 52, p. 355–374.
1299 Symonds, R. B., Reed, M. H., and Rose, W. I., 1992, Origin, speciation, and fluxes of trace-
1300 element gases at Augustine volcano, Alaska: Insights into magma degassing and fumarolic
1301 processes: Geochimica et Cosmochimica Acta, v. 56, p. 633–657.
1302 Symonds, R. B., Rose, W. I., Bluth, G. J., and Gerlach, T. M., 1994, Volcanic-gas studies:
1303 Methods, results, and applications: Reviews in Mineralogy, v. 30, p. 1–66.
1304 Symonds, R. B., Mizutani, Y., and Briggs, P. H., 1996, Long-term geochemical surveillance of
1305 fumaroles at Showa-Shinzan dome, Usu volcano, Japan: Journal of Volcanology and

Hurtig, N. C., Migdisov, A. A., and Williams-Jones, A. E., 2021,
••Are Vapor-Like Fluids Viable Ore Fluids for Cu-Au-Mo Porphyry Ore Formation?
Economic Geology, v. 116, p. 1599-1624.

Geothermal Research, v. 73, p. 177–211.

Tanger, J., and Pitzer, K. S., 1989, Thermodynamics of NaCl-H2O: A new equation of state for the near-critical region and comparisons with other equations for adjoining regions: Geochimica et Cosmochimica Acta, v. 53, p. 973–987.

Taran, Y., and Zelenski, M., 2015, Systematics of water isotopic composition and chlorine content in arc-volcanic gases: Geological Society, London, Special Publications, v. 410, p. 237–262.

Taran, Y. ., Bernard, A., Gavilanes, J. ., Lunezheva, E., Cortez, A., and Armienta, M. A., 2001, Chemistry and mineralogy of high-temperature gas discharges from Colima volcano, Mexico. Implications for magmatic gas- atmosphere interaction: Journal of Volcanology and Geothermal Energy, v. 108, p. 245–264.

Taran, Y. A., Hedenquist, J. W., Korzhinsky, M. A., Tkachenko, S. I., and Shmulovich, K. I., 1995, Geochemistry of magmatic gases from Kudryavy volcano, Iturup, Kuril Islands: Geochimica et Cosmochimica Acta, v. 59, p. 1749–1761.

Taran, Y. A., Bernard, A., Gavilanes, J. C., and Africano, F., 2000, Native gold in mineral precipitates from high-temperature volcanic gases of Colima volcano, Mexico: Applied Geochemistry, v. 15, p. 337–346.

Tarkian, M., Hünken, U., Tokmakchieva, M., and Bogdanov, K., 2003, Precious-metal distribution and fluid-inclusion petrography of the Elatsite porphyry copper deposit, Bulgaria: Mineralium Deposita, v. 38, p. 261–281.

Ulrich, T., and Mavrogenes, J., 2008, An experimental study of the solubility of molybdenum in H2O and KCl-H2O solutions from 500 °C to 800 °C, and 150 to 300 MPa: Geochimica et Cosmochimica Acta, v. 72, p. 2316–2330.

1329 Ulrich, T., Günther, D., and Heinrich, C. A., 1999, Gold concentrations of magmatic brines and
1330 the metal budget of porphyry copper deposits: Nature, v. 399, p. 676–679.
1331 Ulrich, T., Gunther, D., and Heinrich, C. A., 2002, The Evolution of a Porphyry Cu-Au Deposit ,
1332 Based on LA-ICP-MS Analysis of Fluid Inclusions : Bajo de la Alumbrera , Argentina:
1333 Economic Geology, v. 97, p. 1889–1920.
1334 Velizhanin, K. A., Alcorn, C. D., Migdisov, A. A., and Currier, R. P., 2020, Rigorous analysis of
1335 non-ideal solubility of sodium and copper chlorides in water vapor using Pitzer-Pabalan
1336 model: Fluid Phase Equilibria, v. 522, p. 112731.
1337 Vila, T., and Sillitoe, R. H., 1991, Gold-rich porphyry systems in the Maricunga belt, northern
1338 Chile: Economic Geology, v. 86, p. 1238–1260.
1339 Wagner, T., Kulik, D. A., Hingerl, F. F., and Dmytrievava, S. V., 2012, GEM-Selektor
1340 geochemical modeling package: TSolMod library and data interface for multicomponent
1341 phase models: Canadian Mineralogist, v. 50, p. 1173–1195.
1342 Webster, J., 1997, Exsolution of magmatic volatile phases from Cl-enriched mineralizing
1343 granitic magmas and implications for ore metal transport: Geochimica et Cosmochimica
1344 Acta, v. 61, p. 1017–1029.
1345 Webster, J. D., and Botcharnikov, R. E., 2011, Distribution of Sulfur Between Melt and Fluid in
1346 S-O-H-C-Cl-Bearing Magmatic Systems at Shallow Crustal Pressures and Temperatures:
1347 Reviews in Mineralogy and Geochemistry, v. 73, p. 247–283.
1348 Webster, J. D., Sintoni, M. F., and De Vivo, B., 2009, The partitioning behavior of Cl, S, and
1349 H2O in aqueous vapor- ± saline-liquid saturated phonolitic and trachytic melts at 200 MPa:
1350 Chemical Geology, v. 263, p. 19–36.
1351 Weingärtner, H., and Franck, E. U., 2005, Supercritical water as a solvent: Angewandte Chemie

- International Edition, v. 44, p. 2672–2692.

Weis, P., 2015, The dynamic interplay between saline fluid flow and rock permeability in magmatic-hydrothermal systems: Geofluids, v. 15, p. 350–371.

Weis, P., Driesner, T., and Heinrich, C. A., 2012, Porphyry-copper ore shells form at stable pressure-temperature fronts within dynamic fluid plumes: Science, v. 338, p. 1613–1616.

Weis, P., Driesner, T., Coumou, D., and Geiger, S., 2014, Hydrothermal, multiphase convection of H2O-NaCl fluids from ambient to magmatic temperatures: A new numerical scheme and benchmarks for code comparison: Geofluids, v. 14, p. 347–371.

Wendlandt, H. G., and Glemser, V. O., 1964, Reaction of Oxides with Water at High Pressures and Temperatures: Angewandte Chemie - International Edition, v. 309, p. 47–54.

White, J. L., Orr, R. L., and Hultgren, R., 1957, The thermodynamic properties of silver-gold alloys: Acta Metallurgica, v. 5, p. 747–760.

Wilkinson, J. J., 2013, Triggers for the formation of porphyry ore deposits in magmatic arcs: Nature Geoscience, v. 6, p. 917–925.

Williams-Jones, A. E., and Heinrich, C. A., 2005, Vapor transport of metals and the formation of magmatic-hydrothermal ore deposits: Economic Geology, v. 100, p. 1287–1312.

Williams, T. J., Candela, P. A., and Piccoli, P. M., 1997, Hydrogen-alkali exchange between silicate melts and two-phase aqueous mixtures: an experimental investigation: Contributions to Mineralogy and Petrology, v. 128, p. 114–126.

Wood, S., Crerar, D. A., and Borcsik, M., 1987, Solubility of the assemblage pyrite-pyrrhotite-magnetite-sphalerite-galena-gold-stibnite-bismuthinite-argen-tite-molybdenite in H2O-NaCl-CO2 solutions from 200: Economic Geology, v. 82, p. 1864–1887.

Yapparova, A., Miron, G. D., Kulik, D. A., Kosakowski, G., and Driesner, T., 2019, An

advanced reactive transport simulation scheme for hydrothermal systems modelling: Geothermics, v. 78, p. 138–153.

Yin, Y., and Zajacz, Z., 2018, The solubility of silver in magmatic fluids: Implications for silver transfer to the magmatic-hydrothermal ore-forming environment: Geochimica et Cosmochimica Acta, v. 238, p. 235–251.

Zaheri-Abdehvand, N., Tarantola, A., Rasa, I., Hassanpour, S., and Peiffert, C., 2020, Metal content and P-T evolution of CO2-bearing ore-forming fluids of the Haftcheshmeh Cu-Mo porphyry deposit, NW Iran: Journal of Asian Earth Sciences, v. 190.

Zajacz, Z., Halter, W. E., Pettke, T., and Guillong, M., 2008, Determination of fluid/melt partition coefficients by LA-ICPMS analysis of co-existing fluid and silicate melt inclusions: Controls on element partitioning: Geochimica et Cosmochimica Acta, v. 72, p. 2169–2197.

Zajacz, Z., Seo, J. H., Candela, P. A., Piccoli, P. M., Heinrich, C. A., and Guillong, M., 2010, Alkali metals control the release of gold from volatile-rich magmas: Earth and Planetary Science Letters, v. 297, p. 50–56.

Zajacz, Z., Seo, J. H., Candela, P. A., Piccoli, P. M., and Tossell, J. A., 2011, The solubility of copper in high-temperature magmatic vapors: A quest for the significance of various chloride and sulfide complexes: Geochimica et Cosmochimica Acta, v. 75, p. 2811–2827.

Zajacz, Z., Candela, P. A., Piccoli, P. M., Wälle, M., and Sanchez-Valle, C., 2012, Gold and copper in volatile saturated mafic to intermediate magmas: Solubilities, partitioning, and implications for ore deposit formation: Geochimica et Cosmochimica Acta, v. 91, p. 140–159.

Zajacz, Z., Candela, P. A., and Piccoli, P. M., 2017, The partitioning of Cu, Au and Mo between

liquid and vapor at magmatic temperatures and its implications for the genesis of magmatic-hydrothermal ore deposits: Geochimica et Cosmochimica Acta, v. 207, p. 81–101.

Zelenski, M., Malik, N., and Taran, Y., 2014, Emissions of trace elements during the 2012-2013 effusive eruption of Tolbachik volcano, Kamchatka: Enrichment factors, partition coefficients and aerosol contribution: Journal of Volcanology and Geothermal Research, v. 285, p. 136–149.

Zezin, D. Y., Migdisov, A. A., and Williams-Jones, A. E., 2007, The solubility of gold in hydrogen sulfide gas: An experimental study: Geochimica et Cosmochimica Acta, v. 71, p. 3070–3081.

Zezin, D. Y., Migdisov, A. A., and Williams-Jones, A. E., 2011, The solubility of gold in H2O-H2S vapour at elevated temperature and pressure: Geochimica et Cosmochimica Acta, v. 75, p. 5140–5153.

Zhang, L., Audétat, A., and Dolejš, D., 2012, Solubility of molybdenite (MoS2) in aqueous fluids at 600-800 °C, 200 MPa: A synthetic fluid inclusion study: Geochimica et Cosmochimica Acta, v. 77, p. 175–185.

Figure Captions:

Figure 1. (a) Schematic sketch of a porphyry ore deposit modified after Sillitoe (2010), showing the overlapping alteration and ore zones. (b) Illustration of the fluid evolution path along path-A for an intermediate-density vapor dominated pathway and along path-B for a liquid dominated pathway. Phase proportions are calculated using the Lever Rule and the enthalpy-P-X_{NaCl} diagram from Mernagh et al. (2020). (c) Schematic sketches of simulated processes: (1) titration models investigating metal solubility with varying fluid chemistry (S, Cl and redox) at 600 °C and 810

bar, (2) isothermal decompression and (3) isochoric cooling models investigating metal solubility of a fluid with variable composition and (4) single-pass flow-through ore formation models. The fluid is buffered by minerals and saturated with respect to ore forming minerals such as chalcopyrite (ccp), bornite (bor), acanthite (ac), electrum (el) and molybdenite (mo) in models 1 - 3. Buffer-minerals: anh = anhydrite, ru = rutile, mag = magnetite, hem = hematite, py = pyrite, po = pyrrhotite, ilm = ilmenite.

Figure 2. a) Hydration clusters around a gaseous AgCl molecule as a function of increasing water fugacity (AgCl clusters from Godinho et al., 2005). b) Compilation of calculated hydration enthalpy values of various gaseous metal species, NaCl and pure water clusters, see Table 1 for numerical values. Gaseous metallic species show a different correlation of $\Delta H^{298}_{y-1,y}$ with increasing hydration number compared to NaCl.

Figure 3. An experimentally determined solubility isotherm (400 ºC), in which measured gold fugacity normalized to HCl fugacity is shown as a function of water fugacity buffered by the assemblage of molybdenum dioxide-molybdite (blue diamonds). The experimental data were fitted to a power function *f*(x) (red line) for the purpose of extracting integer hydration numbers (y) equivalent to the tangents (dashed red lines) and logarithmic equilibrium constants (K_y).

Figure 4. Compilation of P-T conditions and metal contents in natural low- and intermediate-density fluids from porphyry deposits and in volcanic gas condensates (Table 3). (a) Molybdenum concentrations as a function of temperature and (b) as a function of pressure. (c) Copper concentrations showing a clear correlation with temperature and (d) pressure for Cu below ~4000

Hurtig, N. C., Migdisov, A. A., and Williams-Jones, A. E., 2021,
••Are Vapor-Like Fluids Viable Ore Fluids for Cu-Au-Mo Porphyry Ore Formation?
Economic Geology, v. 116, p. 1599-1624.

ppm. The systematics for Cu could be disturbed due to post-entrapment modification in fluid inclusions. Copper values from single-phase vapor-like and intermediate-density fluid inclusions were accepted if a moderate PT correction reasonable for the respective ore deposit could move the data to intersect the general PT trends. (e) Gold solubility maximum ~500 ºC expressed in the Bingham fluid inclusion data and (f) possible solubility maximum for Au with pressure. (g) Silver concentrations show a positive correlation with temperature mainly expressed by the Mole Granite fluid inclusion data. (h) A temperature-pressure diagram showing the saturation pressure water vapor curve (SPWV – thick black line) with isochores for density lines of pure water (thin black lines) overlaying the vapor-liquid-halite (V+L+H – thick grey line) surface and isochores of the NaCl-H_2O system (thin grey lines) projected onto the PT-surface.

Figure 5. Redox potential (R_H) of various commonly used mineral- and gas-buffers in comparison to R_H simulation traces as a function of isochoric cooling of a fluid with a density of 300 kg/m^3. (a) Redox conditions considered in this study cover a wide range of commonly used mineral-buffers such as the nickel-nickel oxide, the quartz-magnetite-fayalite and the magnetite-hematite buffer. The mineral assemblage of magnetite-anhydrite-rutile typically found as gangue minerals high temperature porphyry allows to define a narrow range of R_H to define the redox potential of porphyry ore-forming fluids. (b) The R_H traces of isochoric cooling models of different starting compositions show that a typical porphyry fluid largely evolves along the H_2S-SO_2 gas buffer, whereas a S-rich fluid may follow the hematite-magnetite and/or pyrite-magnetite buffers.

Figure 6. Chlorine-titration models at 600 °C and 810 bar and ore mineral saturation showing (a, d) the buffering mineralogy, (b, e) the fluid composition and (c, f) the metal ratios. (a) The redox

Hurtig, N. C., Migdisov, A. A., and Williams-Jones, A. E., 2021,
••Are Vapor-Like Fluids Viable Ore Fluids for Cu-Au-Mo Porphyry Ore Formation?
Economic Geology, v. 116, p. 1599-1624.

condition is buffered by the mineral assemblage, magnetite-anhydrite-rutile at low S concentrations (0.2 wt.%) and (d) magnetite-anhydrite-rutile-pyrite at sulfide-saturated conditions (5.5 wt.%). (b, e) The chlorine content correlates positively with Cu, Ag and Au solubility. (c, f) The Ag/Au ratios are relatively constant, whereas the Cu/Au and Cu/Mo ratio increase slightly, and the Mo/Ag ratio decreases with increasing Cl content.

Figure 7. Sulfur-titration models at 600 °C and 810 bar and ore mineral saturation showing (a, d) the buffering mineralogy, (b, e) the fluid composition and (c, f) the metal ratios. The intermediate-density (300 kg/m^3) fluid is mainly buffered by the mineral assemblage magnetite-anhydrite-rutile at lower S contents and becomes saturated with pyrite at ~4.8 wt.% S. The Au and Mo solubility is greatly affected by increasing S content and change by several orders of magnitude.

Figure 8. Redox-titration ($R_H = \log f_{H2}/\log f_{H2O}$) models at 600 °C and 810 bar and ore mineral saturation showing (a, d) the buffering mineralogy, (b-e) the fluid composition and metal ratios. The attention of readers is drawn to the fact that the solubility of the Au chloride and particularly the Au sulfide species reaches a maximum at moderately oxidizing conditions corresponding to those buffered by minerals commonly observed in porphyry systems (i.e., magnetite-anhydrite-rutile).

Figure 9. Results of numerical simulations of metal solubility during isothermal decompression at 600, 400 and 300 °C at varying S content (0.1 and 5.5 wt.%) showing (a-f) metal solubility and (g-j) metal ratios of vapor-like fluids. The attention of readers is drawn to two features in these diagrams. Firstly, there is a strong decrease in the solubility of all the metals with isothermal

Hurtig, N. C., Migdisov, A. A., and Williams-Jones, A. E., 2021,
••Are Vapor-Like Fluids Viable Ore Fluids for Cu-Au-Mo Porphyry Ore Formation?
Economic Geology, v. 116, p. 1599-1624.

decompression and secondly the path of metal solubility for the different fluid compositions changes markedly with temperature.

Figure 10. Results of numerical simulations of metal solubility during isochoric cooling at a density of 100 kg/m^3 and 300 kg/m^3 (isochoric until phase separation, and with further evolution along the saturation pressure water vapor curve, above dashed line). The models were generated for S concentrations of 0.1 wt.% and 5.5 wt.%. (a-d) Metal solubility as a function of temperature, with Au solubility maxima at ~330 ºC in the low-density fluids and at ~450 and ~510 ºC in the intermediate-density fluid. The solubility of Cu, Mo and Ag decreases with decreasing temperature. (e-h) Metal ratios as a function of temperature. The trends for the 0.1 wt.% S and the 5.5 wt.% S models differ considerably.

Figure 11. Single-pass flow-through reactor scheme showing the amounts of ore minerals precipitated during isochoric cooling at a fluid density of 300 kg/m^3 and various starting fluid composition. Metal ratios in starting fluids (a-f) are based on titration models and the degree of undersaturation is similar for all models (Table 4). (a-c) Typical fluid composition for a porphyry ore fluid showing moderate to low Cl contents (500 ppm) as function of increasing S contents (0.5, 1 and 3 wt.% S). With increasing S content, the AuS species become more important, promoting Au transport. (d) The fluid is buffered by the reduced assemblage of magnetite-anhydrite-ilmenite-pyrrhotite at 3 wt.% S. (e-f) Typical fluid composition for a porphyry ore fluid showing high Cl contents (3000 ppm) and increasing S contents (0.1 and 0.5 wt.%). Gold mobility is controlled by the AuCl species and increasing the S content only has a moderate effect on Au transport. (g-h) The excess Cl content was increased to very high HCl/∑Cl ratios comparable to those in volcanic

gases, however the metal concentration was equal to the one used in (f). The models show the sensitivity of metal mobility at a high degree of excess Cl, which moved ore deposition to lower temperatures. Insets show the Au content in electrum (X_{Au} = mole fraction of Au) and the point at which the cumulative precipitation of electrum reaches 98 %. Buffer minerals are: magnetite (Mag), hematite (Hem), Anhydrite (Anh), Rutile (Ru), Ilmenite (Ilm), Calcite (Cal), Pyrite (Py) and Pyrrhotite (Po). Ore minerals are multiplied by a factor to better visualize the ore shells of molybdenite (Mo), acanthite (Acn), bornite (Bor), chalcopyrite (Ccp) and Electrum (El).

Figure 12. The Cu/Au and Mo/Ag ratios of (a) porphyry ore deposits (Singer et al., 2005) compared to (b, c) the simulated metal ratio evolutionary paths from the equilibrium models discussed in 5.1 and 5.2. The simulated metal ratios are determined by metal solubility and represent the capacity of a hydrothermal vapor-like fluid to transport and precipitate metals in a porphyry setting. (b) Metal ratio evolutionary paths from Cl- and redox-titration models, isothermal decompression and isothermal cooling solubility models do not reproduce the general trends of natural porphyry ore deposits. (c) Metal ratio evolutionary metal paths from equilibrium models for variable S content (0 – 10 wt.%), 500 ppm Cl and 0.3 wt.% Cl. At low S content (0 – 1 wt.%), the data follow a vertical trend characterized by decreasing Cu/Au ratios with increasing S content, whereas at elevated S content (1 – 10 wt.%) there is a horizontal trend in which the Mo/Ag ratio decreases with increasing S content. This indicates that the composition of the ore fluid imposes an important control on the ore metal ratios and metal enrichment in porphyry systems.

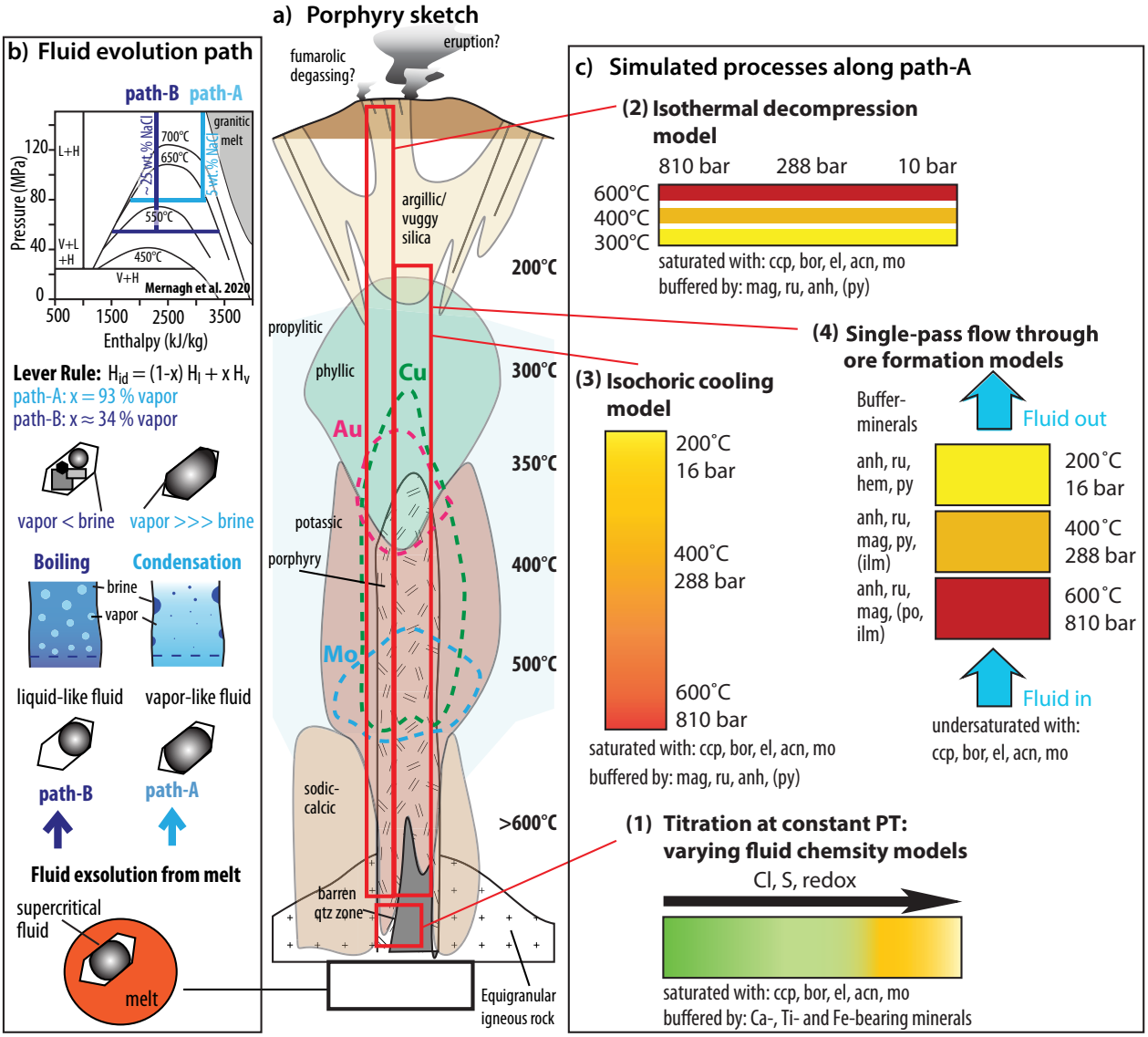

Figure 1

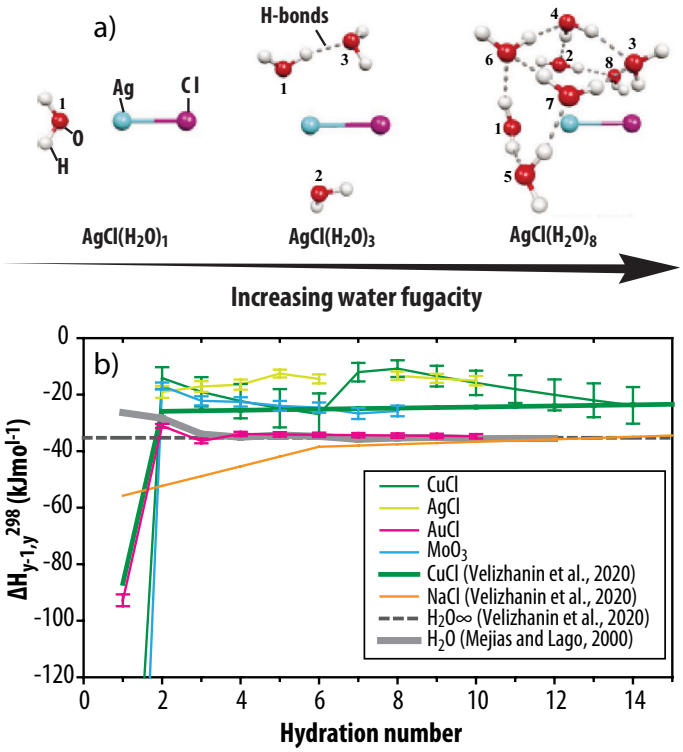

Figure 2

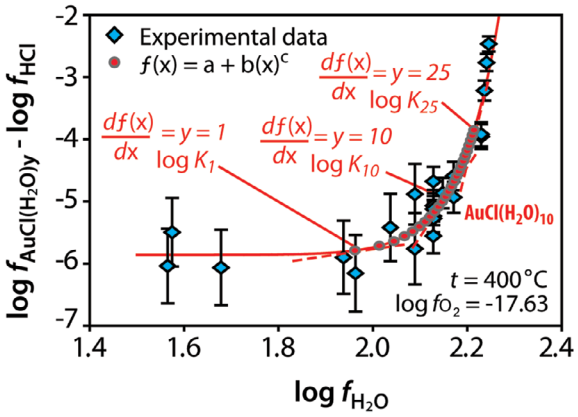

Figure 3

Hurtig, N. C., Migdisov, A. A., and Williams-Jones, A. E., 2021,
••Are Vapor-Like Fluids Viable Ore Fluids for Cu-Au-Mo Porphyry Ore Formation?
Economic Geology, v. 116, p. 1599-1624.

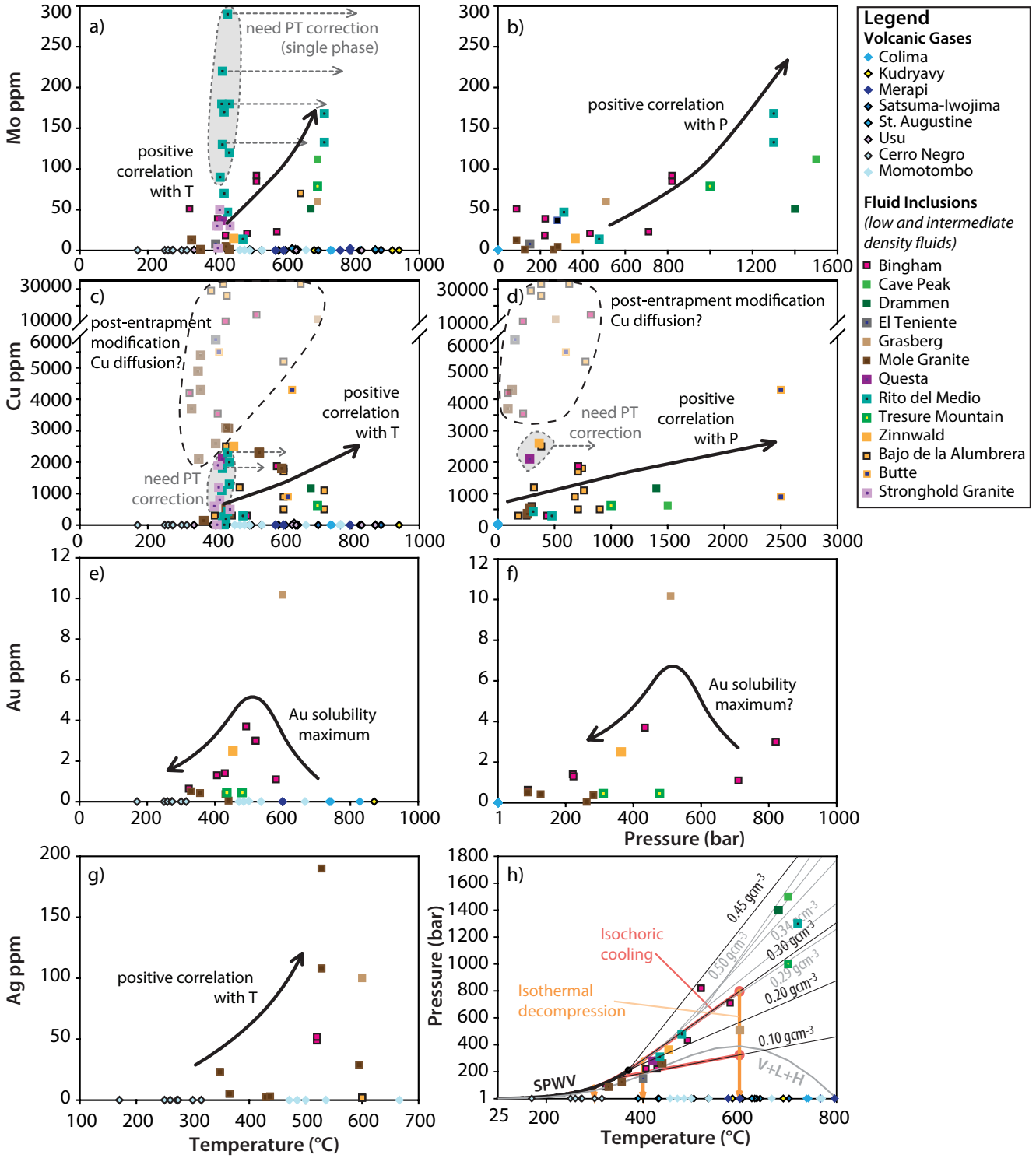

Figure 4

Hurtig, N. C., Migdisov, A. A., and Williams-Jones, A. E., 2021,
••Are Vapor-Like Fluids Viable Ore Fluids for Cu-Au-Mo Porphyry Ore Formation?
Economic Geology, v. 116, p. 1599-1624.

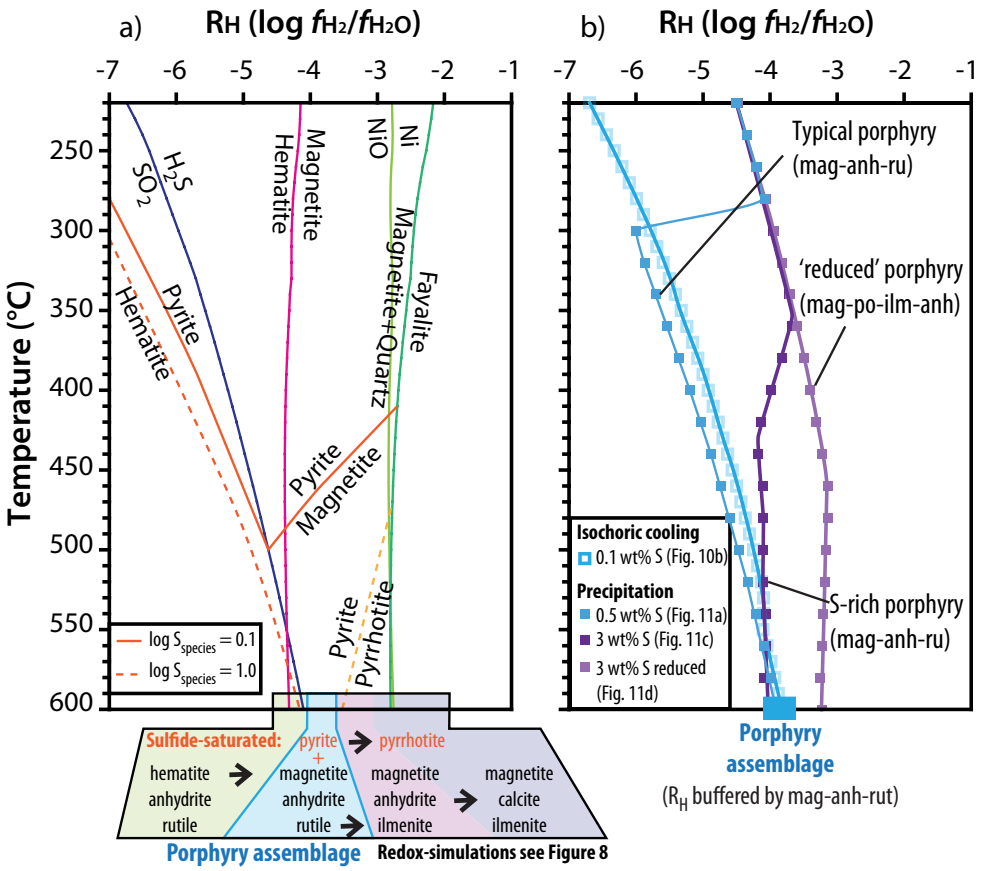

Figure 5

Hurtig, N. C., Migdisov, A. A., and Williams-Jones, A. E., 2021,
••Are Vapor-Like Fluids Viable Ore Fluids for Cu-Au-Mo Porphyry Ore Formation?
Economic Geology, v. 116, p. 1599-1624.

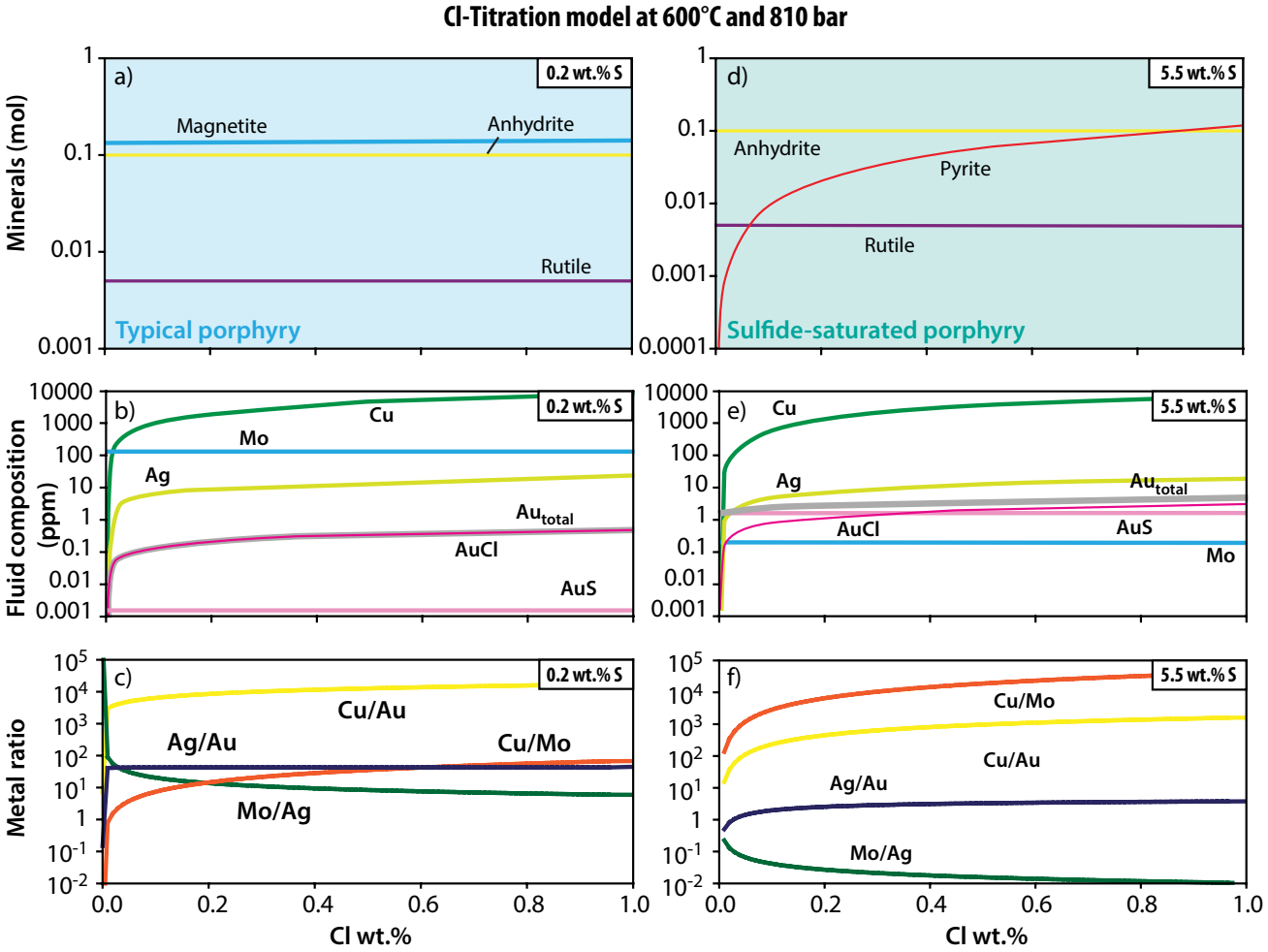

Figure 6

Hurtig, N. C., Migdisov, A. A., and Williams-Jones, A. E., 2021,
••Are Vapor-Like Fluids Viable Ore Fluids for Cu-Au-Mo Porphyry Ore Formation?
Economic Geology, v. 116, p. 1599-1624.

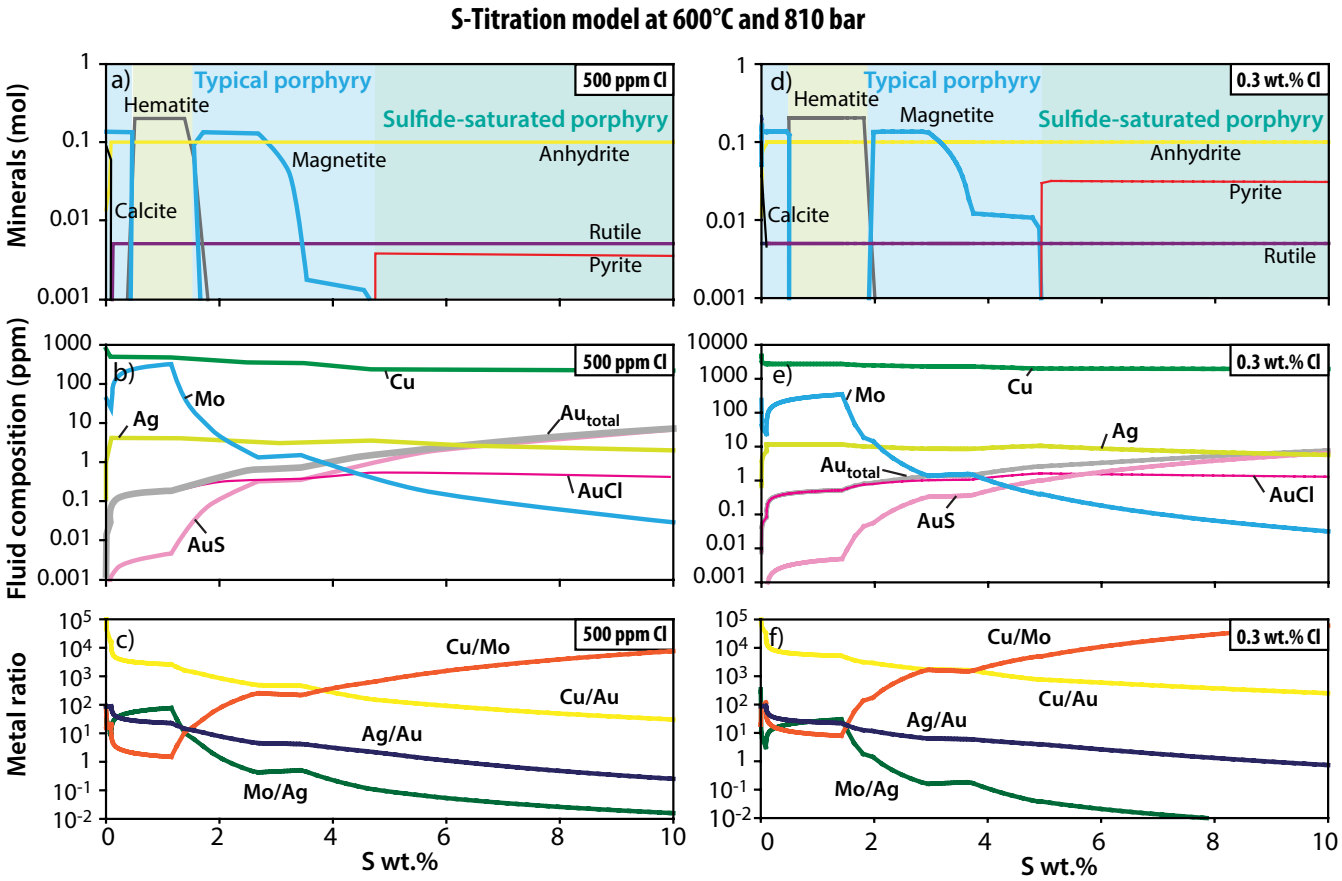

Figure 7

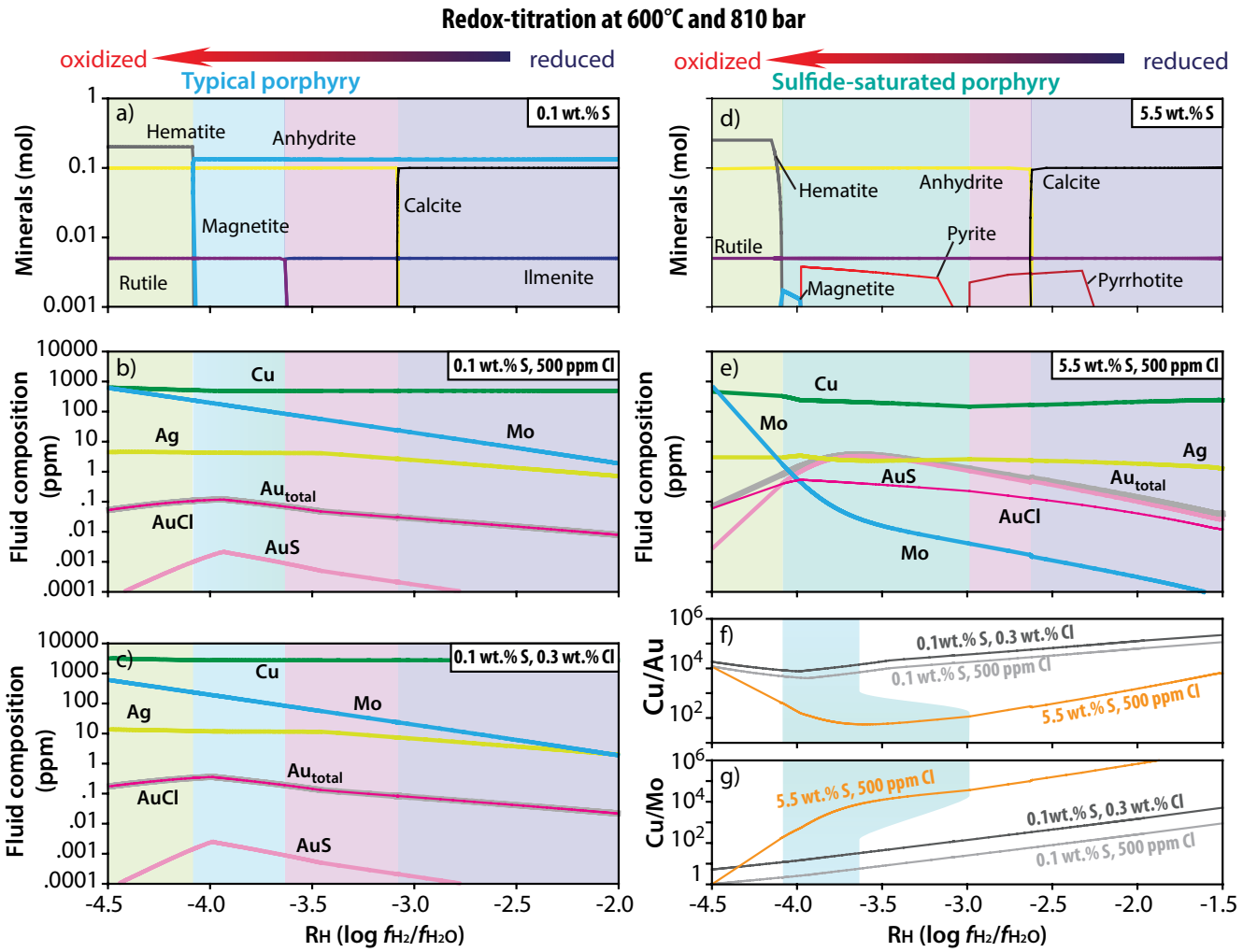

Figure 8

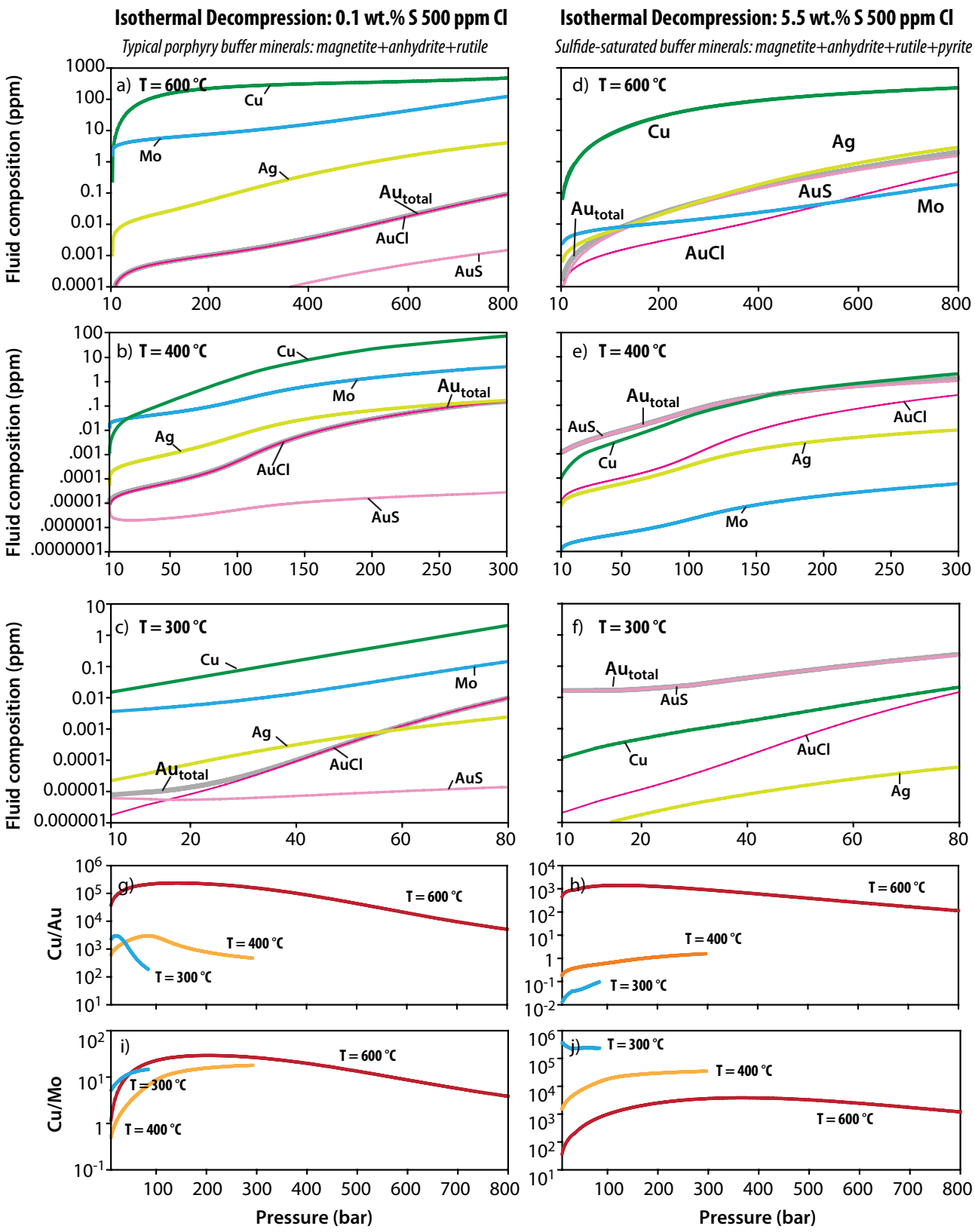

Figure 9

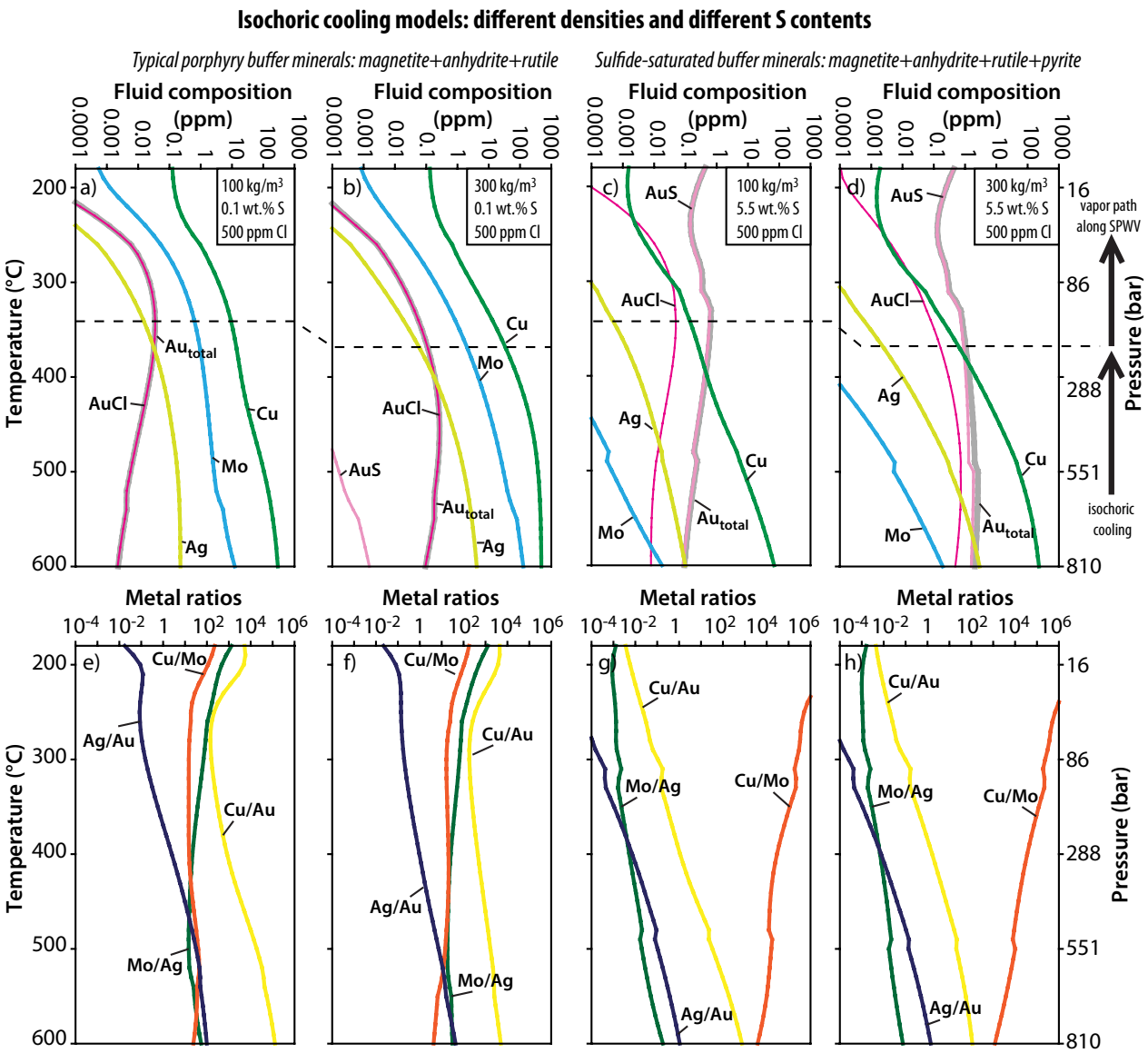

Figure 10

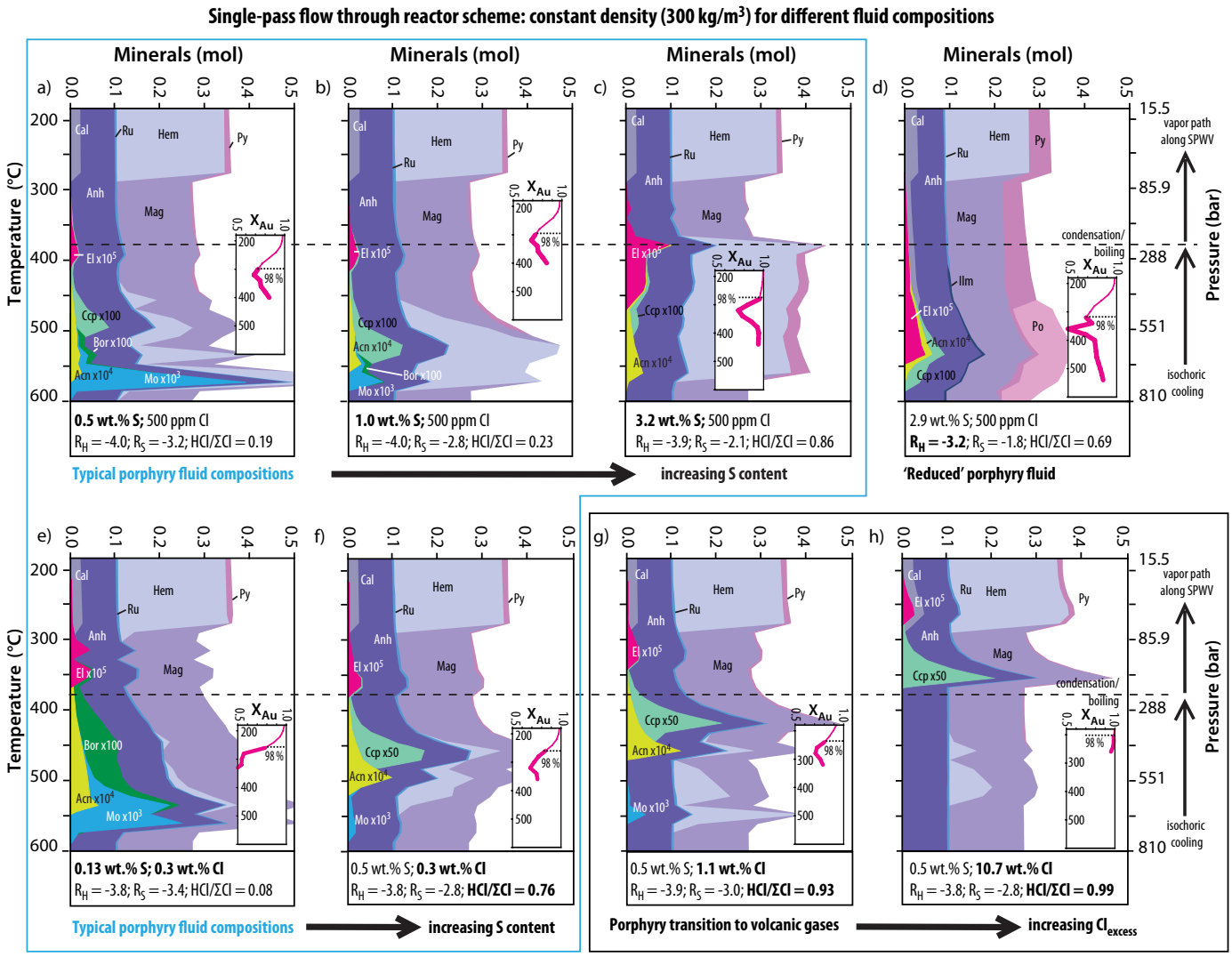

Figure 11

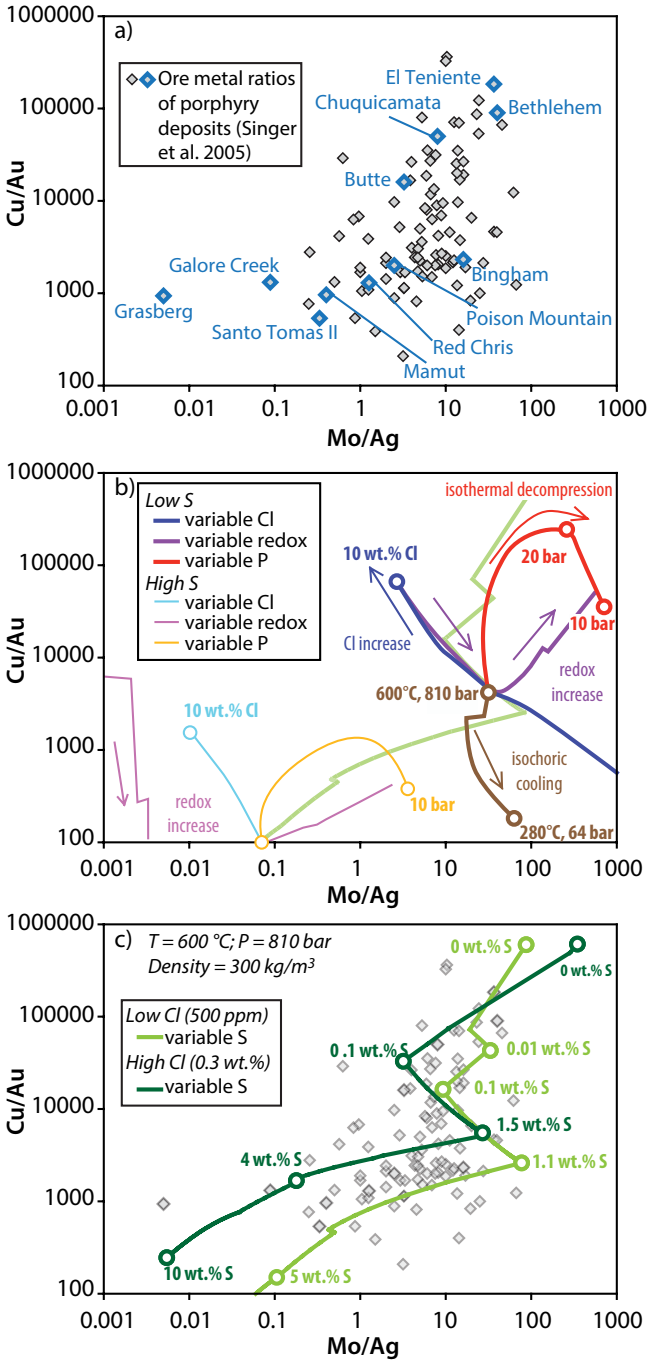

Figure 12

Table 1. Hydration Enthalpy and Entropy for Different Gaseous Metal Species Estimated from Experimental Data Compared to Calculated Density Functional Theory Energies of Water Clusters

Species	Hydration numbers	$H_{y-1,y}^{298}$ (kJmol^{-1})	$S_{y-1,y}^{298}$ (Jmol^{-1}K^{-1})
AuCl[1]	>2	–34.6 ± 0.8	–90.4 ± 1.3
AgCl[2]	>2	–14.8 ± 1.6	–60.8 ± 1.8
CuCl[2]	>2	–19.1 ± 5.2	–66.9 ± 9.2
CuCl[3]	>2	–23.6 ± 1.6	–80.8
NaCl[4]	1–15	–53.13 to –32.42	–91.5
NaCl[3]	1–15	–55.78 to –34.05	–90.2
MoO_3[5]	>2	–24.3 ± 1.8	–76.6 ± 3.6
H_2O[6]	2–12	–26.4 to –35.5	–69.2 to –12.4
H_2O[3]	2 to ∞	–16.6 to –35.3	–79.0 to –11.6

[1]Hurtig and Williams-Jones (2014b)
[2]Calculated, this study
[3]Velizhanin et al. (2020)
[4]Pitzer and Pabalan (1986)
[5]Hurtig and Williams-Jones (2014a)
[6]Mejías and Lago (2000)

Table 2. Numerical Modeling Setup and P-T-x Simulation Conditions

Model	T (°C)	P_{total} (bar)	f_{H_2O} (bar)	Density (kg/m^3)	R_H	Cl (ppm)	S (wt %)	C (wt %)	Ore minerals
Equilibrium models at constant P-T									
Cl titration	600	810	564	300	–3.8 to –3.9	0–10,000	0.2, 5.5	2.0	Saturated
S titration	600	810	564	300	–2.7 to –4.3	500, 3,000	0–10	2.0	Saturated
Redox titration	600	810	564	300	–1.5 to –4.5	500	0.2, 5.5	2.0	Saturated
Cooling and/or decompression models									
Isothermal	600	10–810	8–564	5–300	–3.2 to –3.9	500	0.2, 5.5	2.0	Saturated
decompression	400	10–288	8–174	5–300	–4.5 to –5.1	500	0.02, 4.8	2.0	
	300	10–86	8–68	5–46	–5.6 to –5.9	500	0.002, 3.8	2.0	
Isochoric cooling	180–600		$F_{fH_2O}(T)_{300}$	300	–3.8 to –8.2	500	0.2, 5.5	2.0	Saturated
			$F_{fH_2O}(T)_{100}$	100	–3.8 to –8.4	500	0.2, 5.5		
Single-pass flow-through reactor scheme									
Metal precipitation	180–600		$F_{fH_2O}(T)_{300}$	300	–3.1 to –8.1	500–100,000	3.0, 1.0, 0.1	2.0	Under-saturated at 600°C

For detailed fluid compositions see Appendix 1; $F_{fH_2O}(T)$ = water fugacity as a function of temperature (T) at constant density above the water vapor saturation pressure and then on the saturation pressure water vapor curve; ore minerals: electrum, acanthite, bornite, chalcopyrite, molybdenite (see App. 2 for details)

Table 3. Composition of Natural Volcanic Gases and Low- and Intermediate-Density Fluid Inclusions of Porphyry Deposits

Data	T (°C)	P (bar)	NaCl (wt %)	S (wt %)	Cl (wt %)	C (wt %)	Mo (ppm)	Cu (ppm)	Au (ppm)	Ag (ppm)
Volcanic gases and condensates (references 1–16)										
Minimum	82	~1		0.002	0.002	0.02	0.0006	0.003	7.0×10^{-6}	0.0030
Maximum	1,131	~1		25.6	16.3	55.0	2.80	59.4	0.0050	0.0140
Median	642			1.46	0.49	1.59	0.18	0.30	0.0010	0.0060
Average	646			3.23	1.48	4.01	0.42	3.38	0.0011	0.0084
Standard deviation	150			5.07	2.95	8.51	0.58	10.4	0.0014	0.0048
Number of data points	150			136	146	103	62	64	23	18
Vapor and intermediate density fluid inclusions (references 16–31)										
Minimum	323	2,500	1.0	0.10	0.61	1.07	1.00	10.0	0.05	2.00
Maximum	720	88	8.9	1.25	9.30	13.3	290	4300[1]	10.2	190
Median	431	494	4.4	0.50	2.73	2.00	50.5	850	0.87	23.0
Average	473	649	4.4	0.57	2.85	3.28	71.9	1,116	1.84	42.5
Standard deviation	110	551	2.0	1.47	1.47	2.68	69.3	977	2.50	53.7
Number of data points	68	42	69	24	69	(7[2])	40	46	16	17

1 = Symonds et al. (1987), 2 = Gemmell (1987), 3 = Symonds et al. (1990), 4 = Symonds et al. (1992), 5 = Giggenbach and Matsuo (1991), 6 = Hedenquist e al. (1994), 7 = Symonds et al. (1994), 8 = Taran et al. (1995), 9 = Symonds et al. (1996), 10 = Giggenbach (1996), 11 = Taran et al. (2000, 2001), 12 = Sche et al. (2013), 13 = Zelenski et al. (2014), 14 = Taran and Zelenski (2015, and references therein), 15 = Nadeau et al. (2016), 16 = Ulrich et al. (1999), 17 = Audétat et al. (2000a, b), 18 = Ulrich et al. (2002), 19 = Tarkian et al. (2003), 20 = Rusk et al. (2004), 21 = Redmond et al. (2004), 22 = Klemm et al. (2007 2008), 23 = Seo et al. (2009), 24 = Zajacz et al. (2008), 25 = Rusk et al. (2008), 26 = Audétat, 2010), 27 = Landtwing et al. (2010), 28 = Seo et al. (2012), 2 = Lerchbaumer and Audétat (2013), 30 = Seo and Heinrich (2013), 31 = Audétat (2019); see Appendix 1 for full tables

[1]Cu data were reduced by removing data points that do not follow systematic P-T trends (Fig. 4c, d; App. 1)
[2]Compiled from seven deposits with documented CO_2-bearing inclusions

Table 4. Summary of Starting Fluid Compositions for the Mineral Precipitation Models

Model	S (wt %)	Cl (wt %)	HCl/ΣCl	R_H	R_S	Cu (ppm)	Mo (ppm)	Au (ppm)	Ag (ppm)	Cu/Au	Cu/Mo
11a	0.53	0.05	0.19	–4.0	–3.2	406	65.7	0.09	3.27	4,295	6.2
11b	1.03	0.05	0.23	–4.0	–2.8	380	12.7	0.14	2.62	2,763	30
11c	3.17	0.05	0.86	–3.9	–2.1	65.5	0.21	0.74	3.98	89	318
11d	2.92	0.05	0.69	–3.2	–1.8	144	0.02	0.47	2.18	309	8,169
11e	0.13	0.29	0.08	–3.8	–3.4	2,620	81.3	0.16	8.72	16,624	32
11f	0.50	0.29	0.76	–3.9	–3.0	655	6.27	0.18	7.09	3,694	104
11g	0.50	1.07	0.93	–3.9	–3.0	655	6.37	0.18	7.09	3,694	103
11h	0.50	10.65	0.99	–3.8	–2.8	655	0.09	0.18	7.09	3,694	7,426

Table 5. Summary of Metal Concentrations and Ratios from the Equilibrium Models at 600°C and 810 bar with Varying Fluid Chemistry

Model	S (wt %)	Cl (wt %)	Cu (ppm)	Au (ppm)	Mo (ppm)	Ag (ppm)	Cu/Au	Cu/Mo
Cl titration[1]	0.1	0.01–1.0	0.01–8,817	0.002–0.5	130	0.0002–22	7–17,143	6.0–560,444
Cl titration[2]	5.5	0.01–1.0	27–7,533	1.8–4.7	0.2	0.9–18	15–1,598	135–40,761
S titration[1,2]	0–10	0.05	219–794	0.0001–7.6	0.03–322	0.1–4.2	29–601,871	1.5–8,324
S titration[1,2]	0–10	0.3	1,937 –4,727	0.008–8.2	0.03–344	0.7–11.7	238–611,715	7.9–66,782
Redox titration[1]	0.1	0.05	483–507	0.07–0.12	85–221	4.2–4.3	4,046–6,960	2.3–5.7
Redox titration[1]	0.1	0.3	2,731–2,785	0.2–0.4	80–230	11.6–12.1	7,604–14,910	12–34
Redox titration[2]	5.5	0.05	163–324	0.8–3.7	0.006–1.7	2.3–3.4	55–391	190–25,785

[1]Buffered by the typical porphyry mineral assemblage: magnetite-anhydrite-rutile
[2]Buffered by the sulfide saturated mineral assemblage: pyrite-anhydrite-rutile(-magnetite)